Fall 2013

Harmonic compensation in a grid using doubly fed induction generators

Omkar Amol Ghatpande

Department:

HARMONIC COMPENSATION IN A GRID USING DOUBLY-FED INDUCTION GENERATORS

by

OMKAR AMOL GHATPANDE

A THESIS

Presented to the Faculty of the Graduate School of the

MISSOURI UNIVERSITY OF SCIENCE AND TECHNOLOGY

In Partial Fulfillment of the Requirements for the Degree

MASTER OF SCIENCE IN ELECTRICAL ENGINEERING

2013

Approved by

Mehdi Ferdowsi

Keith Corzine

Jonathan Kimball

ABSTRACT

Ideally, electric utilities are expected to deliver a sinusoidal voltage with a constant rated frequency, while customers are expected to draw a sinusoidal current with unity power factor. The recent widespread use of harmonic producing equipment in industrial applications, especially non-linear loads, has increased the distortion of electric currents and voltages in transmission and distribution systems. This thesis proposes a method of using multiple reference frame theory for measuring and mitigating harmonic currents of nonlinear loads using a doubly fed induction generator. The most significant low-order harmonics to be compensated are calculated using a multiple reference frame harmonic observer. This observer is simulated using Matlab® Simulink® and then implemented using the Texas Instruments TMS320F28335 digital signal processor. Experimental and simulation results are provided to verify the analysis of the observer by comparing the results with calculations from the Fourier spectrum. Along with active and reactive power generation, an algorithm is proposed to inject currents in the rotor for the mitigation of $6n \pm 1$ harmonics in the system. Simulation results are presented to demonstrate the performance of this proposed method. These results validate the effectiveness of the method in compensating the targeted harmonics in the system. This method of measuring and compensating harmonics discussed in this thesis is accurate, straightforward, easily implemented and effective in the mitigation of any harmonic in the system. The currents obtained in the fundamental reference frame can be further employed for the control of active and reactive power flow.

ACKNOWLEDGMENTS

I would like to express my sincere gratitude to my advisors, Dr. Mehdi Ferdowsi and Dr. Keith Corzine. Their vision and guidance have provided a good basis for the present thesis. I would like to sincerely thank Dr. Jonathan Kimball, for his constant support and for serving on my thesis committee.

This thesis would not have been possible without the guidance and the help of several individuals who extended their valuable assistance. I really appreciate all my fellow lab mates and students in power group in assisting me. Thanks are also due to my friends in Rolla and back in India.

I am obliged to my loving family Aai, Baba, Kaka, Kaku, Lalit, Shubhamkar in India. Without their encouragement, sacrifice and moral support pursuing Master's Degree would be a dream for me. Last but not the least, to the one above all of us, the omnipresent God, for answering all my prayers and blessing me.

Also I would mention that this research was sponsored by the Department of Energy under the grant DE-EE0002012.

TABLE OF CONTENTS

Page

LIST OF ILLUSTRATIONS

Page

LIST OF TABLES

NOMENCLATURE

DFIG	Doubly-Fed Induction Generator
MRF	Multiple Reference Frame
MRFHO	Multiple Reference Frame Harmonic Observer
THD	Total harmonic Distortion
CF	Crest Factor
v_{abcs}, v_{abcr}	Stator and rotor side voltages in abc variables
i_{abcs}, i_{abcr}	Stator and rotor side currents in abc variables
v_{qd0s}, v_{qd0r}	qd0 axis stator and rotor voltages
i_{qd0s}, i_{qd0r}	qd0 axis stator and rotor currents
λ_{abcs}, λ_{abcr}	Stator and rotor side flux linkages
v'_{abcr}, i'_{abcr}	qd0 axis rotor side voltage and currents referred to stator side
P, Q	Active and reactive power
p	derivative $\frac{\mathrm{d}}{\mathrm{d}t}$
N_s, N_r	Stator and Rotor turns
θ_r	actual rotor position
ω_r	Rotor Speed
r_s, r_r	Stator and Rotor resistance
r'_r	Referred rotor resistance
P_p	Pole pairs
T_e	Electrical Torque
J	Rotor and connected load Inertia
T_L	Load Torque
i^n_{qd0}	qd0 axis current in n^{th} reference frame

1. INTRODUCTION

1.1. MOTIVATION AND THESIS OUTLINE

Ideally, electric utilities are expected to deliver a sinusoidal voltage with a constant rated frequency, while customers are also expected to draw a sinusoidal current with unity power factor. Electrical power distribution systems are experiencing increase in the amount of distorted current due to the use of non-linear power electronic loads in industrial and commercial applications. In this thesis, a multiple reference frame based harmonic measurement and compensation method is proposed.

Section one discusses the current global wind energy scenario, different types of wind turbines, and power quality issues with detailed analysis of harmonics in the power system. Section two covers the development of the model of a doubly fed induction generator (DFIG) and the simulation results of the standalone DFIG model.

Section three covers the measurement of harmonics using the multiple reference frame theory. A simulation model for the multiple reference frame theory based harmonic observer is discussed. This simulation model is modified to implement this observer on a Texas Instruments TMS320F28335 digital signal processor using Embedded Coder of Matlab. Simulation results and experimental results are presented for various cases.

Section four covers the multiple reference frame theory harmonic compensation for a DFIG. Simulation results are presented for harmonic compensation. Section five introduces a technique for the independent control of active, reactive power, and harmonic compensation.

1.2. WIND ENERGY SCENARIO

In the last couple of decades, there has been a significant improvement in wind turbine technology which has maximized energy conversion, reduced costs and incorporated ancillary services like reactive power compensation, and power quality improvement. Global installed capacity of wind turbine based electric generation is significantly growing as shown in Figure 1.1. Current installed capacity has reached 282,275 MW and expected to exceed 500 GW and 1,000 GW by the year 2016 and 2020 respectively. All wind turbines currently can provide more than 3% of the global electricity demand [1].

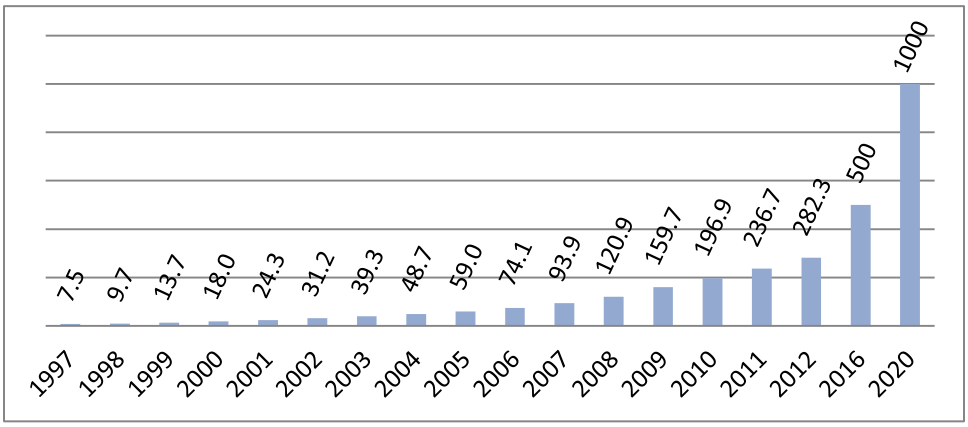

Figure 1.1. Total World Installed Capacity (GW) [1]

1.3. WIND TURBINE CONFIGURATIONS

Due to the recent developments in the electrical and mechanical aspects of wind turbine systems, the size and electrical generation capacity of individual wind generators are rapidly increasing as seen in Figure 1.2. Wind turbines are classified based on parameters like mechanical power regulation (pitch control or stall control) or drive train

configuration (geared drive or direct drive system). However, in the market for wind turbine based electricity generation, they are popularly classified based on their rotor speed mainly Fixed Speed and Variable Speed turbine configurations.

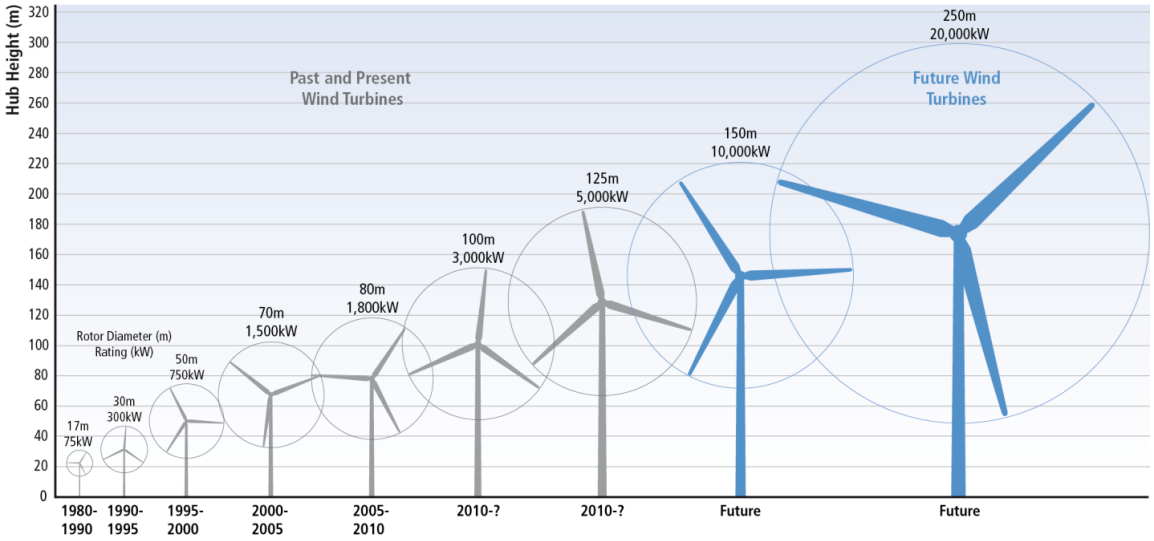

Figure 1.2. Wind Turbine Size [2]

1.3.1. Fixed Speed Turbine Configuration. Fixed speed turbine configurations use a multistage gearbox and a squirrel cage induction generator which is directly connected to the grid through a transformer. For fixed speed systems, stall control or pitch control for the blades are used. Sometimes to widen the speed range of the turbine, pole changeable induction generators are used.

In 1980s and 1990s, most of wind turbines installed were stall controlled fixed speed turbines. This type of configuration is also known as the 'Danish concept'. The rotor blades are permanently fixed on the hub, so the construction of this type is relatively simple. The blades are adjusted only once when the system is erected. This angle is selected to maximize energy capture after a study of wind speed profiles of the area.

Figure 1.3 shows the block diagram for configuration of fixed speed type of wind turbines connected to the grid.

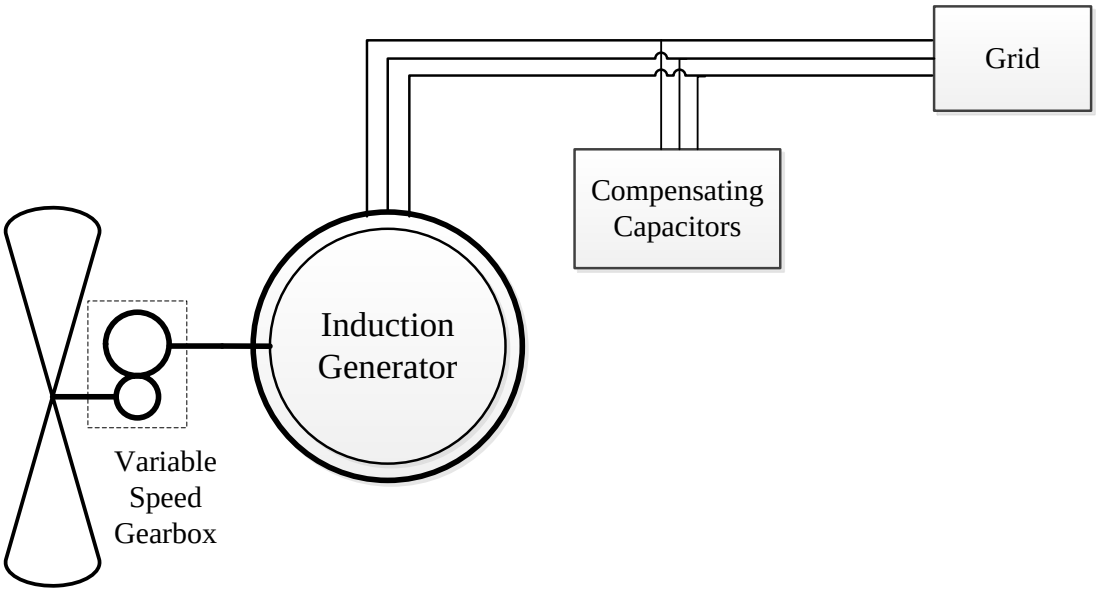

Figure 1.3. Fixed Speed Turbine Configuration

The main advantage of a fixed speed configuration is that it is robust, easy and relatively cheap for mass production, and also it does not have any electrical connection between the stator and the rotor [3]. Due to single adjustment of the blade, the efficiency of the turbine is variable over the wind speed range. Main disadvantages for the fixed speed turbines are

- Fixed speed wind turbines have a very small wind speed range at which they operate at high efficiency.
- Wind fluctuations cause electromechanical torque transients which exerts mechanical stress on the turbine and the drive train components.
- Tower shadowing effect and shear effect cause flicker in the power generated.
- A multistage gearbox in the fixed speed turbines which is very costly and heavy.

1.3.2. Variable Speed Configuration. The variable speed configuration has a generator, a multistage gear box, and most importantly a power electronic converter. This converter helps generate a constant power at constant voltage and frequency. The main reason of using a variable speed configuration is to improve energy capture, reduce stresses on drive train, and increase power quality. For obtaining this, the high cost of the power electronic converter has to be invested.

There are many different kinds of wind turbine systems which employ variable rotor speed. In the configuration shown in the Figure 1.4, all the power generated by the wind generator passes through the power electronic converter. So this converter has to be rated at the nominal generator rating. The generator used can be either a squirrel cage induction generator or a permanent magnet synchronous generator.

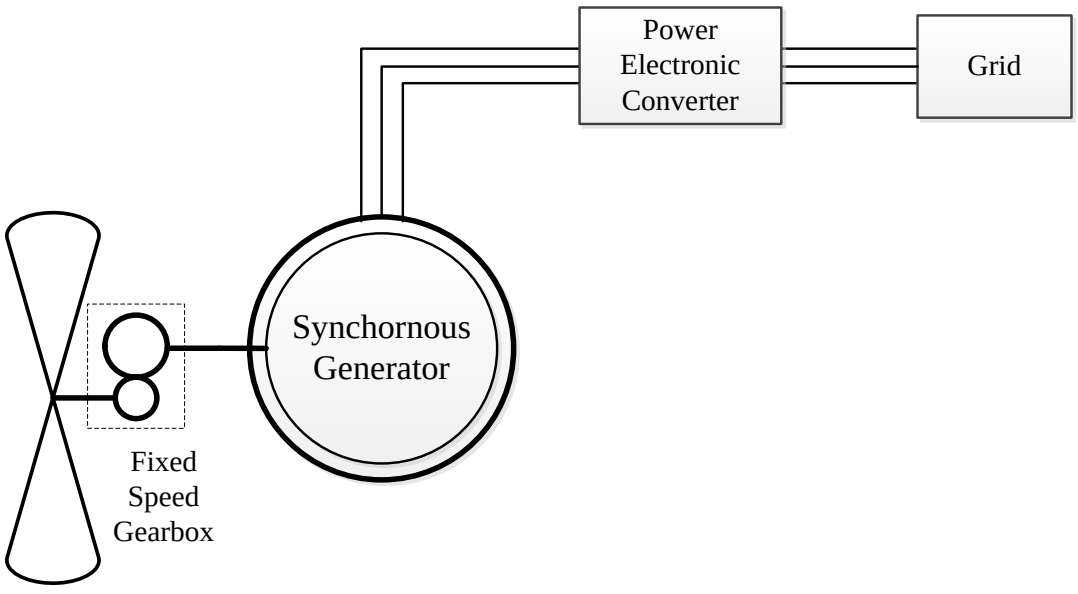

Figure 1.4. Direct Drive Synchronous Machine

Advantages for both machines are that they are slightly cheaper, brushless, and can be used for grids frequency of 50 Hz or 60 Hz. As all generated power passes through the power converter, there are some additional losses in the converter.

1.4. DOUBLY-FED INDUCTION GENERATOR BASED (DFIG) WIND ENERGY SYSTEMS

The DFIG system is a viable alternative for variable speed over a range at minimal investment. So currently it is the preferred choice generator for medium and high capacity wind turbines. The DFIG system can operate over a wide speed range in both sub synchronous as well as super synchronous speeds. Figure 1.5 shows the block diagram of DFIG based wind turbine system.

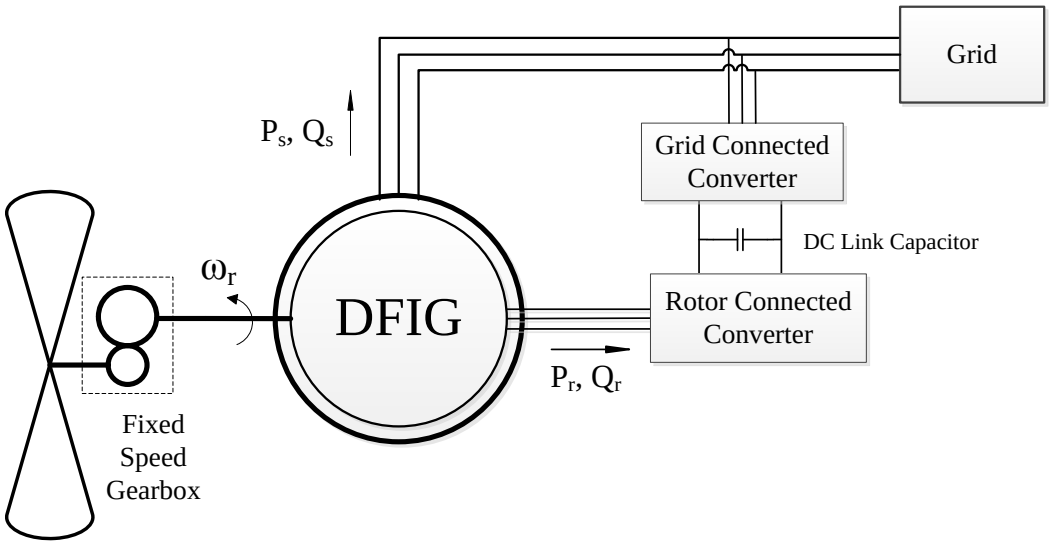

Figure 1.5. Doubly-Fed Induction Generator Based Wind Turbine Configuration

1.4.1. Configuration. The stator circuit is directly connected to the grid while the rotor is connected to a rotor-side three-phase bi-directional power converter via a slip ring configuration. The power rating of the rotor-side converter decides the permissible speed variation for the wind turbine. For the systems where speed range requirement is small, the rotor-side converter is rated at 25-30% of the nominal generator power. The other side of the converter is connected to a DC link capacitor. The DC link voltage is maintained constant by a grid connected power converter.

1.4.2. Advantages. The main advantages of the DFIG system are

- The rotor speed can be variable within a range of $\pm$30% of the synchronous speed[4].
- The power electronic converter handles only a fraction (25–30%) of the total power. So the losses in the converter are reduced.
- With proper modeling and control algorithms, independent control of the active and reactive power is possible. Also advanced control strategies like harmonic compensation can be implemented.
- Reduction in the cost of the converter and the variable speed gearbox.

1.4.3. Disadvantages. The main disadvantages of the DFIG system are

- The rotor is connected to the converter via slip rings which have high wear and tear and require frequent maintenance.
- The speed range of the generator in limited on the rating of the converter.
- As gearbox is used, it adds to the investment, weight, and energy losses.

1.5. ELECTRIC POWER QUALITY

Power quality is broadly defined as any abnormalities or disturbances in the power supply system. The power quality issue includes different problems like transients, sags or surges, voltage imbalances, power outages, distortions in the waveform, EMI noise, etc. In terms of power quality and harmonic current distortion, IEEE 519 [5] and IEC EN 61000-3 [6] standards specify the required regulations governing harmonic compliance for a typical power distribution systems.

1.5.1. Harmonics. The current drawn by a nonlinear load when connected to a sinusoidal power source is non-sinusoidal. The reason for the non-sinusoidal current drawn may be physical properties of the load or the switching action of the power electronic switches. These load side harmonic currents interact with the utility power impedance and produce voltage and current distortions. For analyzing these harmonic current or voltages, they are mathematically expressed as a summation of sinusoidal waves having frequencies as integral multiples of the fundamental frequency. Fourier series analysis is used to decompose the distorted periodic waveform.

$$f(t) = a_0 + \sum_{n=1}^{\infty} \left(a_n \cos n\omega_1 t + b_n \sin n\omega_1 t \right) \tag{1}$$

where

$$a_0 = \frac{1}{T} \int_0^T f(t)\,\mathrm{d}t \tag{2}$$

$$a_n = \frac{2}{T} \int_0^T f(t) \cos n\omega_1 t \mathrm{d}t \tag{3}$$

$$b_n = \frac{2}{T}\int_0^T f(t)\sin n\omega_1 t dt \tag{4}$$

Term a_0 is usually the average value where T is the period of function *f*. Here we see that the Fourier series extends till infinity. But in practice the value of n is limited to some higher order harmonic. The symmetry of waveforms will be an even function if the value of b_n is zero. Similarly the symmetry of waveforms will be an odd function if the value of a_n is zero. The rms (root mean square) value of the distorted current or voltage waveform in terms of fundamental and harmonic current is given by

$$f_{rms}^2 = f_{rms_1}^2 + f_{rms_3}^2 + f_{rms_5}^2 + f_{rms_7}^2 + \ldots\ldots \tag{5}$$

$$f_{rms}^2 = f_{rms_1}^2 + f_{rms_H}^2 \tag{6}$$

Figure 1.6 shows the waveforms for the 1st, 3rd, 5th and 7th harmonic frequencies.

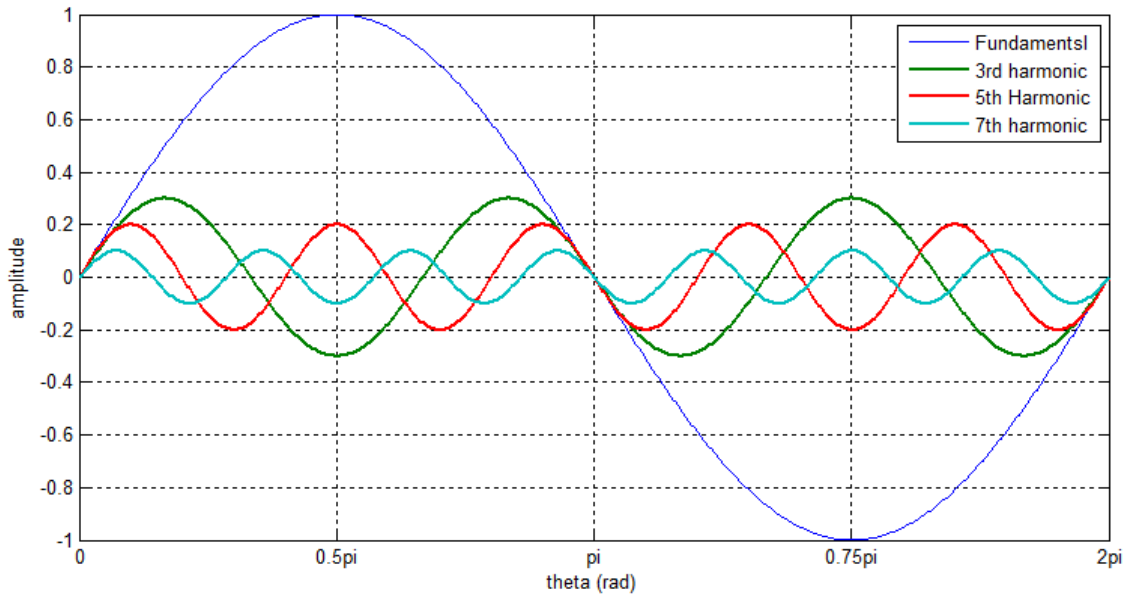

Figure 1.6. Waveforms of Fundamental and Harmonic Frequencies

The most common way of measuring a distorted waveform is by calculating its total harmonic distortion (THD). It is the ratio of the rms value of the harmonic component to the rms value of the fundamental component of the wave.

$$THD = \frac{f_{rms_H}}{f_{rms_1}} \tag{7}$$

Another way of measuring distortion is by calculating the crest factor for the waveform which is defined as the ratio of the peak value to the rms value. If the value of crest factor is other than 1.414, then it indicates there is distortion in the waveform.

$$C.F. = \frac{f_{\max}}{f_{rms}} \tag{8}$$

Any n^{th} harmonic can be analyzed using the theory of symmetrical components. Phase Sequence of positive sequence is defined to have same phase rotation as the fundamental waveform. Similarly negative sequence will have opposite rotation. Zero sequence will have all the phases in the same direction. As shown in Table 1.1, phase sequence of the fundamental wave is A-B-C. The harmonics of the order 6n+1 (7th, 13th, etc.) will rotate in a forward direction or with positive sequence while 6n-1 harmonics (5th, 11th, etc.) will rotate in a backward direction or with negative sequence. Table 1.1 illustrates the phase sequence of different odd harmonics.

Table 1.1. Phase Sequence for Harmonic Currents

Phase	**A**	**B**	**C**	**Phase Sequence**
Fundamental	0°	120°	240°	A-B-C
3rd harmonic	$3\times0^\circ=0^\circ$ 0°	$3\times120^\circ=360^\circ$ $360^\circ=0^\circ$	$3\times240^\circ=720^\circ$ $360^\circ=0^\circ$	no rotation
5th harmonic	$5\times0^\circ=0^\circ$ 0°	$5\times120^\circ=600^\circ$ $600^\circ-720^\circ=-120^\circ$	$5\times240^\circ=1200^\circ$ $1200^\circ-1080^\circ=120^\circ$	A-C-B
7th harmonic	$7\times0^\circ=0^\circ$ 0°	$7\times120^\circ=840^\circ$ $840^\circ-720^\circ=120^\circ$	$7\times240^\circ=1680^\circ$ $1680^\circ-1440^\circ=240^\circ$	A-B-C

1.5.2. Harmonics Producing Equipment. Consumers have the most control over the generation of harmonic currents as their equipment and systems draws non sinusoidal current from the source. The main sources of harmonics are the power electronics equipment like variable voltage supplies, switch mode power supplies, arc furnaces, battery chargers, variable speed drives, inverters etc. Depending on the switching time and duty ratio the current harmonics in the power electronic equipment would vary.

1.5.3. Effect of Harmonics. Some of the major effects of current harmonics in power lines are greater power losses in distribution systems, overheating, lower power factor, interference problems in communication systems and possible failures of sensitive electronic equipment. Due to triplen harmonics there might be overcurrent in neutral wire of distribution system. Highly distorted current waveforms have a very low power factor. If the natural resonant frequency of the capacitor bank present in the power system equals to the frequency of one of the n^{th} harmonic current, very high voltage distortions can produced by the capacitor bank. Also there might be false tripping of circuit breakers due to high values of harmonic currents.

Negative sequence harmonics produces torque in the opposite directions of positive sequence harmonics. So harmonics like 5^{th} 13^{th} etc. will oppose the rotation of the induction motor. This not only causes torque fluctuations but also reduces the service life of motors. Harmonics cause excessive losses in induction as well as synchronous motors.

Harmonic currents interact with impedance in the system and give rise to voltage harmonics. The amount by which the voltage will distort depends not only on the harmonic current magnitude but also the power system impedance. Maximum harmonics will be produced when high magnitudes of harmonic currents are injected into a weak bus or when the impedance is very large. The voltage drop of V_{hn} in the system due to harmonic currents is given by

$$V_{hn} = Z_s \sum_{n=3,5,7}^{\infty} I_n \sin\left(n\omega_1 t + \theta_n\right) \tag{9}$$

The voltage at the load bus is given by

$$V_{load} = V_s - I_1 Z_s \sin\left(\omega_1 t + \theta_1\right) - Z_s \sum_{n=3,5,7}^{\infty} I_n \sin\left(n\omega_1 t + \theta_n\right) \tag{10}$$

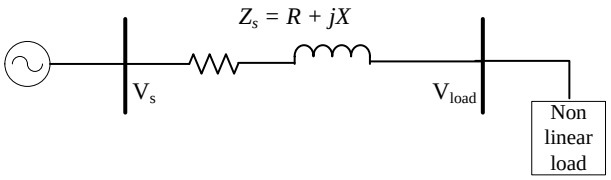

Figure 1.7. Voltage Distortions Due To Harmonic Currents in a Grid

1.6. HARMONIC COMPENSATION TECHNIQUES

Most of the current solutions for harmonic mitigation are based on the following basic options [7]

- Reduction of harmonic currents produced due to non-sinusoidal loads.
- Modifying the frequency response of power system by the use of filters or passive elements like capacitors or inductors.
- Using filters to absorb or block harmonic currents.

Many methods are employed to modify the power system response to the harmonics. The most economical way is to remove the capacitor in the system. But this can lead to a lower power factor, hence higher distribution losses, and lower bus voltage. So either the size of the capacitor or the location of the capacitor can be changed. Adding shunt filter can be used to change the system response.

The most common way for harmonic mitigation is designing a harmonic filter which is tuned to absorb or block the harmonic frequency distorting the system. Firstly, a

harmonic analysis is done to find the most troublesome frequency and accordingly a passive filter is designed which mainly consists of resistive, capacitive and inductive elements. Passive filters could be either single tuned or higher order high pass configurations. The main problem of such design is that it does not respond to the changes in the magnitude of current harmonic and it compensates only the harmonics for which it has been designed.

To overcome the disadvantages of passive filters, Active Power filters are used to mitigate the harmonic distortions. Along with passive elements, Active Power filters use modern semiconductor devices and advanced electronic circuits like digital signal processors, hall effect sensors, operational and isolation amplifiers[8]. A lot of research has been conducted in harmonic measurement techniques and power electronic device control techniques.

2. MODELING OF DOUBLY FED INDUCTION GENERATOR

2.1. MATHEMATICAL MODELING OF DOUBLY FED INDUCTION GENERATOR

Doubly-fed induction generator is essentially a wound rotor induction machine. Induction machines are the most extensively used electric machines in the industries for energy conversion between electrical and mechanical energies. This is because of their rugged and reliable performance. The winding arrangement for the 2 pole, 3-phase, wye-connected symmetrical induction machine is shown in Figure 2.1 [9].

The following assumptions were made while developing this model

- Friction and windage losses are negnected
- Iron losses are neglected
- Magnetic saturation is not considered
- Skin effect is neglected

2.1.1. Stator And Rotor Equations In Machine Variables. The stator windings are identical, sinusoidally distributed windings, displaced by 120° with N_s equivalent turns and winding resistance per phase r_s . Likewise the rotor windings are also identical, sinusoidally distributed windings, displaced by 120° with N_r equivalent turns and winding resistance per phase r_r . In all equations subscript *s* indicates to all the parameters and variables related to stator circuit while *r* indicates to all the parameters and variables related to rotor circuit. The voltage equations in machine variables is expressed as

$$v_{abcs} = r_s i_{abcs} + p\lambda_{abcs} \tag{11}$$

$$v_{abcr} = r_r i_{abcr} + p\lambda_{abcr} \tag{12}$$

where

$$p = \frac{\mathrm{d}}{\mathrm{d}t}$$

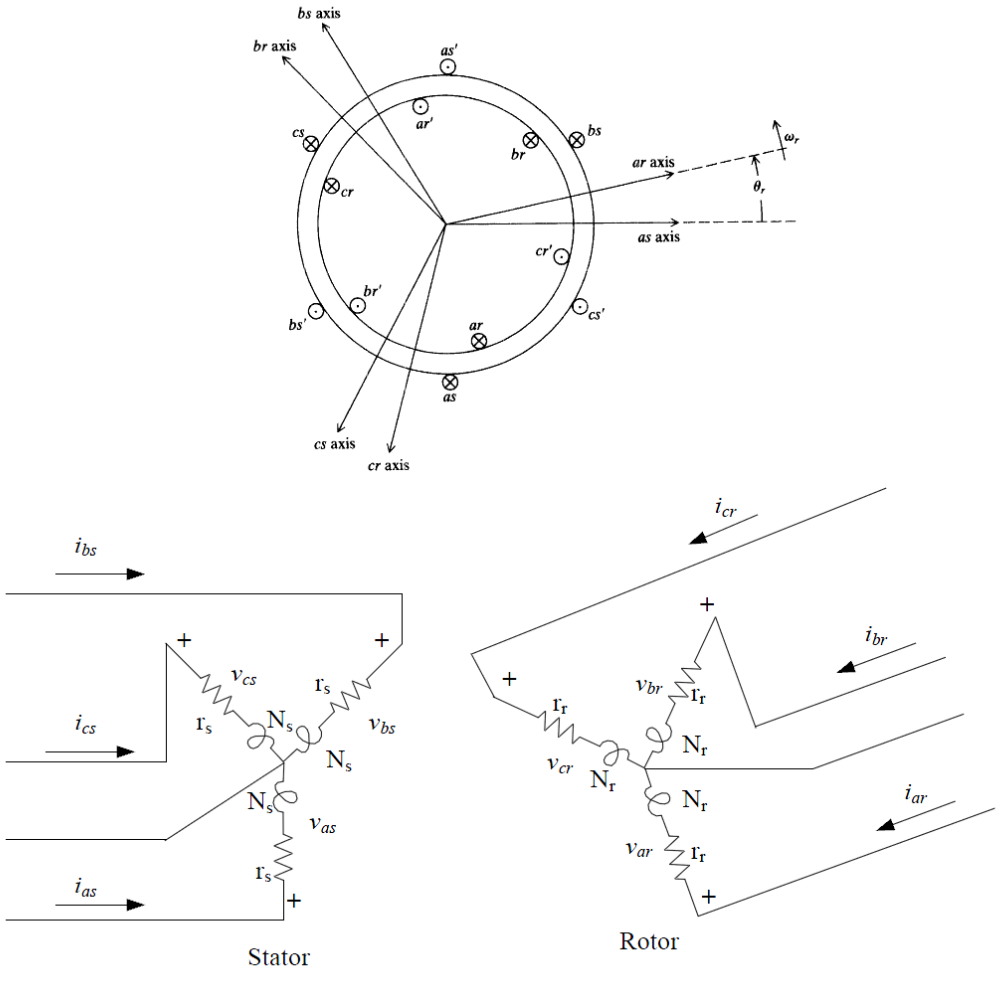

Figure 2.1. Two Pole, 3-phase, Wye Connected Symmetrical Induction Machine.

$$f_{abcs} = \begin{bmatrix} f_{as} \\ f_{bs} \\ f_{cs} \end{bmatrix} \quad \text{and} \quad f_{abcr} = \begin{bmatrix} f_{ar} \\ f_{br} \\ f_{cr} \end{bmatrix} \tag{13}$$

In equation(13), f can represent any variable namely voltage, current, flux linkage etc. For magnetically linear systems, the flux linkage may be expressed as

$$\begin{bmatrix} \lambda_{abcs} \\ \lambda_{abcr} \end{bmatrix} = \begin{bmatrix} L_s & L_{sr} \\ (L_{sr})^T & L_r \end{bmatrix} \begin{bmatrix} i_{abcs} \\ i_{abcr} \end{bmatrix} \tag{14}$$

The winding inductances L_s, L_r, L_{sr} are defined as,

$$L_s = \begin{bmatrix} L_{ls} + L_{ms} & -\frac{1}{2}L_{ms} & -\frac{1}{2}L_{ms} \\ -\frac{1}{2}L_{ms} & L_{ls} + L_{ms} & -\frac{1}{2}L_{ms} \\ -\frac{1}{2}L_{ms} & -\frac{1}{2}L_{ms} & L_{ls} + L_{ms} \end{bmatrix} \tag{15}$$

where

$$L_{ls} = \frac{N_s^2}{R_{ls}},\ L_{ms} = \frac{N_s^2}{R_m}$$

$$L_r = \begin{bmatrix} L_{lr} + L_{ms} & -\frac{1}{2}L_{mr} & -\frac{1}{2}L_{mr} \\ -\frac{1}{2}L_{mr} & L_{lr} + L_{mr} & -\frac{1}{2}L_{mr} \\ -\frac{1}{2}L_{mr} & -\frac{1}{2}L_{mr} & L_{lr} + L_{mr} \end{bmatrix} \tag{16}$$

where

$$L_{lr} = \frac{N_r^2}{R_{lr}},\ L_{mr} = \frac{N_r^2}{R_m}$$

$$\mathrm{L_{sr}} = L_{sr}\begin{bmatrix} \cos(\theta_r) & \cos\left(\theta_r + \frac{2\pi}{3}\right) & \cos\left(\theta_r - \frac{2\pi}{3}\right) \\ \cos\left(\theta_r - \frac{2\pi}{3}\right) & \cos(\theta_r) & \cos\left(\theta_r + \frac{2\pi}{3}\right) \\ \cos\left(\theta_r + \frac{2\pi}{3}\right) & \cos\left(\theta_r - \frac{2\pi}{3}\right) & \cos(\theta_r) \end{bmatrix} \quad (17)$$

In equations (15) and(16), L_{ls} and L_{ms} are leakage and magnetizing inductances of stator windings, while L_{lr} and L_{mr} are leakage and magnetizing inductances of rotor windings respectively. In equation (17) inductance L_{sr} is amplitude of mutual inductances between stator and rotor whereas θ_r is the actual rotor position. All rotor variables are referred to the stator windings by appropriate turns ratio as it is convenient to express the voltage equations in machine variable form.

$$i'_{abcr} = \frac{N_r}{N_s} i_{abcr} \quad (18)$$

$$v'_{abcr} = \frac{N_s}{N_r} v_{abcr} \quad (19)$$

$$\lambda'_{abcr} = \frac{N_s}{N_r} \lambda_{abcr} \quad (20)$$

The magnetizing and mutual inductances are associated with same magnetic flux path therefore L_{ms}, L_{mr}, L_{sr} are related as

$$L_{ms} = \frac{N_s}{N_r} L_{sr} \quad (21)$$

The mutual inductance between stator and rotor are now defined as

$$L_{sr}^{'} = \frac{N_s}{N_r} L_{sr} = L_{ms} \begin{bmatrix} \cos(\theta r) & \cos\left(\theta r + \frac{2\pi}{3}\right) & \cos\left(\theta r - \frac{2\pi}{3}\right) \\ \cos\left(\theta r - \frac{2\pi}{3}\right) & \cos(\theta r) & \cos\left(\theta r + \frac{2\pi}{3}\right) \\ \cos\left(\theta r + \frac{2\pi}{3}\right) & \cos\left(\theta r - \frac{2\pi}{3}\right) & \cos(\theta r) \end{bmatrix} \quad (22)$$

$$L_{mr} = \left(\frac{N_r}{N_s}\right)^2 L_{ms} \text{ and } L_r^{'} = \left(\frac{N_r}{N_s}\right)^2 L_r$$

So the rotor inductance from equation (16)

$$L_r^{'} = \begin{bmatrix} L_{lr}^{'} + L_{ms} & -\frac{1}{2}L_{mr} & -\frac{1}{2}L_{mr} \\ -\frac{1}{2}L_{mr} & L_{lr}^{'} + L_{mr} & -\frac{1}{2}L_{mr} \\ -\frac{1}{2}L_{mr} & -\frac{1}{2}L_{mr} & L_{lr}^{'} + L_{mr} \end{bmatrix} \quad (23)$$

where

$$L_{lr}^{'} = \left(\frac{N_s}{N_r}\right)^2 L_{lr}$$

The flux linkages can be now expressed as

$$\begin{bmatrix} \lambda_{abcs} \\ \lambda_{abcr}^{'} \end{bmatrix} = \begin{bmatrix} L_s & L_{sr}^{'} \\ \left(L_{sr}^{'}\right)^T & L_r^{'} \end{bmatrix} \begin{bmatrix} i_{abcs} \\ i_{abcr}^{'} \end{bmatrix} \quad (24)$$

The voltage equations expressed in terms of machine variables referred to the stator windings may be written as

$$\begin{bmatrix} v_{abcs} \\ v'_{abcr} \end{bmatrix} = \begin{bmatrix} r_s + pL_s & pL'_{sr} \\ p\left(L'_{sr}\right)^T & r'_r + pL'_r \end{bmatrix} \begin{bmatrix} i_{abcs} \\ i'_{abcr} \end{bmatrix} \tag{25}$$

where

$$r'_r = \left(\frac{N_s}{N_r}\right)^2 r_r$$

The torque and rotor speed are related by

$$T_e = JP_p p\omega_r + T_L \tag{26}$$

In the above equation, J is the rotor inertia and sometimes the connected load is also considered in the inertia, also P_p represents pole pairs in stator and ω_r is rotor speed. The load torque T_L is positive for a torque load on the shaft of the induction machine.

2.1.2. Equations of Transformation for Stator Circuit. Change of variables is used in analyzing an electrical machine to eliminate different time varying quantities like inductances in ac machine. The machine inductances are functions of rotor speed. Park Transformation is many times used to eliminate the time varying variables like machine inductances by either using a stationary reference frame or some particular or arbitrary angular velocity.

Transformation of voltage equations to arbitrary reference frame or any particular reference frame will reduce the complexity of the voltage differential equations.

Applying Park's Transformation

$$f_{qd0s} = K_s f_{abcs} \tag{27}$$

where

$$f_{qd0s} = \begin{bmatrix} f_{qs} \\ f_{ds} \\ f_{0s} \end{bmatrix}$$

and f_{abcs} is as defined in equation (13)

$$K_s = \frac{2}{3}\begin{bmatrix} \cos(\theta) & \cos\left(\theta - \frac{2\pi}{3}\right) & \cos\left(\theta + \frac{2\pi}{3}\right) \\ sin(\theta) & \sin\left(\theta - \frac{2\pi}{3}\right) & \sin\left(\theta + \frac{2\pi}{3}\right) \\ \frac{1}{2} & \frac{1}{2} & \frac{1}{2} \end{bmatrix} \tag{28}$$

The inverse of K_s is given as

$$(K_s)^{-1} = \begin{bmatrix} \cos(\theta) & sin(\theta) & 1 \\ \cos\left(\theta - \frac{2\pi}{3}\right) & \sin\left(\theta - \frac{2\pi}{3}\right) & 1 \\ \cos\left(\theta + \frac{2\pi}{3}\right) & \sin\left(\theta + \frac{2\pi}{3}\right) & 1 \end{bmatrix} \tag{29}$$

The arbitrary angular velocity ω and the angular displacement θ is related by

$$\theta = \int \omega \cdot \mathrm{d}t \tag{30}$$

where θ is any arbitrary angle.

2.1.3. Equations Of Transformation For Rotor Circuit. Applying Park's Transformation to rotor circuit

$$f'_{qd0r} = K_r f'_{abcr} \tag{31}$$

where,

$$f'_{qd0r} = \begin{bmatrix} f'_{qr} \\ f'_{dr} \\ f'_{0r} \end{bmatrix} \quad \text{and} \quad f'_{abcr} = \begin{bmatrix} f'_{ar} \\ f'_{br} \\ f'_{cr} \end{bmatrix}$$

$$K_r = \frac{2}{3}\begin{bmatrix} \cos(\beta) & \cos\left(\beta - \frac{2\pi}{3}\right) & \cos\left(\beta + \frac{2\pi}{3}\right) \\ sin(\beta) & \sin\left(\beta - \frac{2\pi}{3}\right) & \sin\left(\beta + \frac{2\pi}{3}\right) \\ \frac{1}{2} & \frac{1}{2} & \frac{1}{2} \end{bmatrix} \tag{32}$$

The inverse of K_r is given as

$$(K_r)^{-1} = \begin{bmatrix} \cos(\beta) & sin(\beta) & 1 \\ \cos\left(\beta - \frac{2\pi}{3}\right) & \sin\left(\beta - \frac{2\pi}{3}\right) & 1 \\ \cos\left(\beta + \frac{2\pi}{3}\right) & \sin\left(\beta + \frac{2\pi}{3}\right) & 1 \end{bmatrix} \tag{33}$$

If rotor angular displacement is given by θr given by

$$\omega_r = \frac{d\theta_r}{\mathrm{d}t}$$

and the arbitrary angle β is defined as

$$\beta = \theta - \theta r$$

2.1.4. Voltage Equations In Arbitrary Reference Frame. Transforming equations (11) and (12) by applying Park's Transformation. Stator voltage equations will be

$$v_{qd0s} = r_s i_{qd0s} + \omega\lambda_{dqs} + p\lambda_{qd0s} \tag{34}$$

where

$$\lambda_{dqs} = \begin{bmatrix} \lambda_{ds} \\ -\lambda_{ds} \\ 0 \end{bmatrix}$$

Rotor voltage equations will be

$$v'_{qd0r} = r'_r i'_{qd0r} + (\omega - \omega_r)\lambda'_{dqr} + p\lambda'_{qd0r} \tag{35}$$

where

$$\lambda'_{dqr} = \begin{bmatrix} \lambda'_{dr} \\ -\lambda'_{qr} \\ 0 \end{bmatrix}$$

The flux linkage equation for stator and rotor can be written as

$$\lambda_{abcs} = L_s i_{abcs} + L'_{sr} i'_{abcr} \tag{36}$$

$$\lambda'_{abcr} = \left(L'_{sr}\right)^T i_{abcs} + L'_r i'_{abcr} \tag{37}$$

Above flux linkage equations will be transformed to

$$\lambda_{qd0s} = K_s\ L_s \left(K_s\right)^{-1} i_{qd0s} + K_s\ L'_{sr} \left(K_r\right)^{-1} i'_{qd0r} \tag{38}$$

$$\lambda'_{qd0r} = K_r \left(L'_{sr}\right)^T \left(K_s\right)^{-1} i_{qd0s} + K_r \; L'_r \left(K_r\right)^{-1} i'_{qd0r} \tag{39}$$

Above flux linkage equations and be simplified to write in a matrix form as

$$\begin{bmatrix} \lambda_{qd0s} \\ \lambda'_{qd0r} \end{bmatrix} = \begin{bmatrix} K_s \; L_s \left(K_s\right)^{-1} & K_s \; L'_{sr} \left(K_r\right)^{-1} \\ K_r \left(L'_{sr}\right)^T \left(K_s\right)^{-1} & K_r \; L'_r \left(K_r\right)^{-1} \end{bmatrix} \begin{bmatrix} i_{qd0s} \\ i'_{qd0r} \end{bmatrix} \tag{40}$$

In equation (40) the value of terms in the matrix using Park's transformation can be simplified to

$$K_s \; L_s \left(K_s\right)^{-1} = \begin{bmatrix} L_{ls} + L_m & 0 & 0 \\ 0 & L_{ls} + L_m & 0 \\ 0 & 0 & L_{ls} + L_m \end{bmatrix} \tag{41}$$

$$K_r \; L'_r \left(K_r\right)^{-1} = \begin{bmatrix} L'_{lr} + L_m & 0 & 0 \\ 0 & L'_{lr} + L_m & 0 \\ 0 & 0 & L'_{lr} + L_m \end{bmatrix} \tag{42}$$

$$K_s \; L'_{sr} \left(K_r\right)^{-1} = K_r \left(L'_{sr}\right)^T \left(K_s\right)^{-1} = \begin{bmatrix} L_m & 0 & 0 \\ 0 & L_m & 0 \\ 0 & 0 & L_m \end{bmatrix} \tag{43}$$

where,

$$L_M = \frac{3}{2} L_{ms}$$

Voltage equations for stator in qd0 variables can be expanded by substituting above flux equations and written as

$$v_{qs} = r_s i_{qs} + \omega \; \lambda_{ds} + p\lambda_{qs} \tag{44}$$

$$v_{ds} = r_s i_{ds} - \omega \; \lambda_{qs} + p\lambda_{ds} \tag{45}$$

$$v_{0s} = r_s i_{0s} + p\lambda_{0s} \tag{46}$$

where,

$$\lambda_{qs} = L_{ls} i_{qs} + L_m \left(i_{qs} + i_{qr}^{'} \right) \tag{47}$$

$$\lambda_{ds} = L_{ls} i_{ds} + L_m \left(i_{ds} + i_{dr}^{'} \right) \tag{48}$$

$$\lambda_{0s} = L_{ls} i_{0s} \tag{49}$$

Similarly voltage equations for rotor are written as

$$v_{qr}^{'} = r_r^{'} i_{qr}^{'} + (\omega - \omega_r)\lambda_{dr}^{'} + p\lambda_{qr}^{'} \tag{50}$$

$$v_{dr}^{'} = r_r^{'} i_{dr}^{'} - (\omega - \omega_r)\lambda_{qr}^{'} + p\lambda_{dr}^{'} \tag{51}$$

$$v_{0r}^{'} = r_r^{'} i_{0r}^{'} + p\lambda_{0r}^{'} \tag{52}$$

where,

$$\lambda_{qr}^{'} = L_{lr}^{'} i_{qr}^{'} + L_m \left(i_{qs} + i_{qr}^{'} \right) \tag{53}$$

$$\lambda_{dr}^{'} = L_{lr}^{'} i_{dr}^{'} + L_m \left(i_{ds} + i_{dr}^{'} \right) \tag{54}$$

$$\lambda_{0r}^{'} = L_{lr}^{'} i_{0r}^{'} \tag{55}$$

The torque in $qd0$ variable is given by many equations such as

$$T_e = \left(\frac{3}{2} \right) \left(\frac{P}{2} \right) \left(\lambda_{qs} i_{qs} - \lambda_{ds} i_{ds} \right) \tag{56}$$

$$T_e = \left(\frac{3}{2} \right) \left(\frac{P}{2} \right) \left(\lambda_{qr}^{'} i_{dr}^{'} - \lambda_{dr}^{'} i_{qr}^{'} \right) \tag{57}$$

Because machine and power system parameters are nearly always given in ohms or in per unit of base impedance, it is convenient to express the voltage and flux linkage equations in terms of reactance rather than inductances. In the equations ω_b is base electrical angular velocity, Ψ is flux linkage per second

$$v_{qs} = r_s i_{qs} + \frac{\omega}{\omega_b}\Psi_{ds} + \frac{p}{\omega_b}\Psi_{qs} \tag{58}$$

$$v_{ds} = r_s i_{ds} - \frac{\omega}{\omega_b}\Psi_{qs} + \frac{p}{\omega_b}\Psi_{ds} \tag{59}$$

$$v_{0s} = r_s i_{0s} + \frac{p}{\omega_b}\Psi_{0s} \tag{60}$$

where,

$$\Psi_{qs} = X_{ls} i_{qs} + X_m \left(i_{qs} + i'_{qr} \right) \tag{61}$$

$$\Psi_{ds} = X_{ls} i_{ds} + X_m \left(i_{ds} + i'_{dr} \right) \tag{62}$$

$$\Psi_{0s} = X_{ls} i_{0s} \tag{63}$$

Similarly voltage equations for rotor are written as

$$v'_{qr} = r'_r i'_{qr} + \frac{(\omega - \omega_r)}{\omega_b}\Psi'_{dr} + \frac{p}{\omega_b}\Psi'_{qr} \tag{64}$$

$$v'_{dr} = r'_r i'_{dr} - \frac{(\omega - \omega_r)}{\omega_b}\Psi'_{qr} + \frac{p}{\omega_b}\Psi'_{dr} \tag{65}$$

$$v'_{0r} = r'_r i'_{0r} + \frac{p}{\omega_b}\Psi'_{0r} \tag{66}$$

where,

$$\Psi'_{qr} = X'_{lr} i'_{qr} + X_m \left(i_{qs} + i'_{qr} \right) \tag{67}$$

$$\Psi'_{dr} = X'_{lr} i'_{dr} + X_m \left(i_{ds} + i'_{dr} \right) \tag{68}$$

$$\Psi'_{0r} = X'_{lr} X'_{0r} \tag{69}$$

and inductive reactance is calculated by product of base speed and inductance

$$X_k = \omega_b L_k \tag{70}$$

2.1.5. Modified Voltage equations for Computer Simulations. For developing the equations for computer simulations firstly stator and rotor current are calculated by rearranging Equations (51-53), (57-59) and solving for currents

$$i_{qs} = \frac{1}{X_{ls}} \left(\Psi_{qs} - \Psi_{mq} \right) \tag{71}$$

$$i_{ds} = \frac{1}{X_{ls}} \left(\Psi_{ds} - \Psi_{md} \right) \tag{72}$$

$$i_{0s} = \frac{\Psi_{0s}}{X_{ls}} \tag{73}$$

$$i'_{qr} = \frac{1}{X'_{lr}} \left(\Psi'_{qr} - \Psi_{mq} \right) \tag{74}$$

$$i'_{dr} = \frac{1}{X'_{lr}} \left(\Psi'_{dr} - \Psi_{md} \right) \tag{75}$$

$$i'_{0r} = \frac{\Psi'_{0r}}{X'_{lr}} \tag{76}$$

where,

$$\Psi_{mq} = X_m \left(i_{qs} - i'_{qr} \right)$$

$$\Psi_{md} = X_m \left(i_{ds} - i'_{dr} \right)$$

For developing the voltage equations for computer simulations the voltage equations are rearranged such derivatives operation is modified to integral sign to solve for the flux linkages per second.

$$\Psi_{qs} = \int \left(\omega_b v_{qs} - \omega \Psi_{ds} - \frac{r_s \omega_b (\Psi_{qs} - \Psi_{mq})}{X_{ls}} \right) \tag{77}$$

$$\Psi_{ds} = \int \left(\omega_b v_{ds} + \omega \Psi_{qs} - \frac{r_s \omega_b (\Psi_{ds} - \Psi_{md})}{X_{ls}} \right) \tag{78}$$

$$\Psi_{0s} = \int \omega_b \left(v_{0s} - \frac{r_s \Psi_{0s}}{X_{ls}} \right) \tag{79}$$

$$\Psi'_{qr} = \int \left(\omega_b v'_{qr} - (\omega - \omega_r) \Psi'_{dr} - \frac{r'_r \omega_b (\Psi'_{qr} - \Psi_{mq})}{X'_{lr}} \right) \tag{80}$$

$$\Psi'_{dr} = \int \left(\omega_b v'_{dr} + (\omega - \omega_r) \Psi_{qs} - \frac{r'_r \omega_b (\Psi'_{dr} - \Psi_{md})}{X'_{lr}} \right) \tag{81}$$

$$\Psi'_{0r} = \int \omega_b \left(v'_{0r} - \frac{r'_r \Psi'_{0r}}{X'_{lr}} \right) \tag{82}$$

where,

$$\Psi_{mq} = X_{aq} \left(\frac{\Psi_{qs}}{X_{ls}} - \frac{\Psi'_{qr}}{X'_{lr}} \right) \tag{83}$$

$$\Psi_{md} = X_{ad}\left(\frac{\Psi_{ds}}{X_{ls}} - \frac{\Psi'_{dr}}{X'_{lr}}\right) \tag{84}$$

$$X_{ad} = X_{aq} = \left(\frac{1}{X_m} + \frac{1}{X_{ls}} + \frac{1}{X'_{lr}}\right)^{-1} \tag{85}$$

The torque in qd0 variable is given by many equations such as

$$T_e = \left(\frac{3}{2}\right)\left(\frac{P}{2}\right)\left(\frac{1}{w_b}\right)\left(\Psi_{ds} i_{qs} - \Psi_{qs} i_{ds}\right) \tag{86}$$

By rearranging equation (26) rotor speed is calculated as

$$\omega_r = \int \frac{\sum TP_p}{J} \mathrm{d}t \tag{87}$$

where $\sum T$ gives the summation of all torques

Active and reactive power is calculated by

$$P = \left(\frac{3}{2}\right)\left(v_{qs} i_{qs} + v_{ds} i_{ds} + v_{0s} i_{0s}\right) \tag{88}$$

$$Q = \left(\frac{3}{2}\right)\left(v_{qs} i_{qs} - v_{ds} i_{ds}\right) \tag{89}$$

2.2. COMPUTER SIMULATION MODEL

The computer simulation is done Matlab Simulink. The block diagram for induction machine simulation is as shown in Figure 2.2.

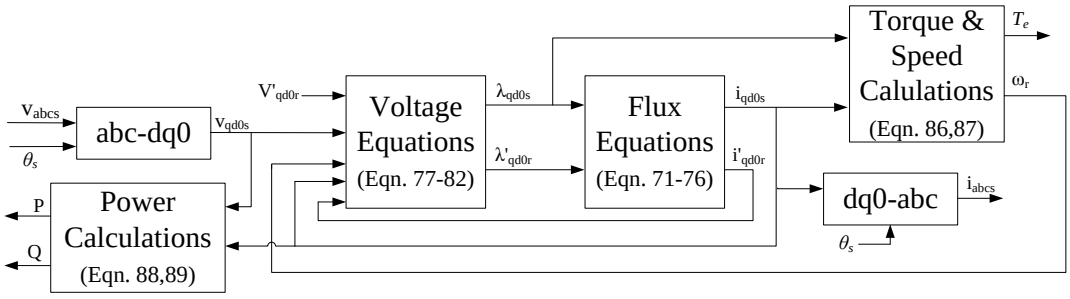

Figure 2.2. Block Diagram of Induction Machine Simulation

Simulink model is developed as shown in Figure 2.3 according to the block diagram in Figure 2.2. The inputs to the subsystem 'Round Rotor Induction Motor' are stator voltage, rotor voltage and rotor speed calculated from mechanical equations. The applied stator voltage is transformed to dq0 parameters. For squirrel cage rotor, the voltage applied will be 0. In case of DFIG the controller will calculate the injected rotor voltage. Actual rotor speed is calculated by using the mechanical equation(87). The machine parameters and constants are defined in an m-file which has to be executed before the execution of the Simulink model.

Table 2.1. Induction Machine Parameters [9]

Power (HP)	Power (KW)	Volts	rpm	T_B (N.m)	I_B (amps)
50	37.28	460	1705	198	46.8
r_s (Ω)	X_{ls} (Ω)	X_m (Ω)	X'_{lr} (Ω)	r'_r (Ω)	J (kg.m^2)
0.087	0.302	13.08	0.302	0.228	1.662

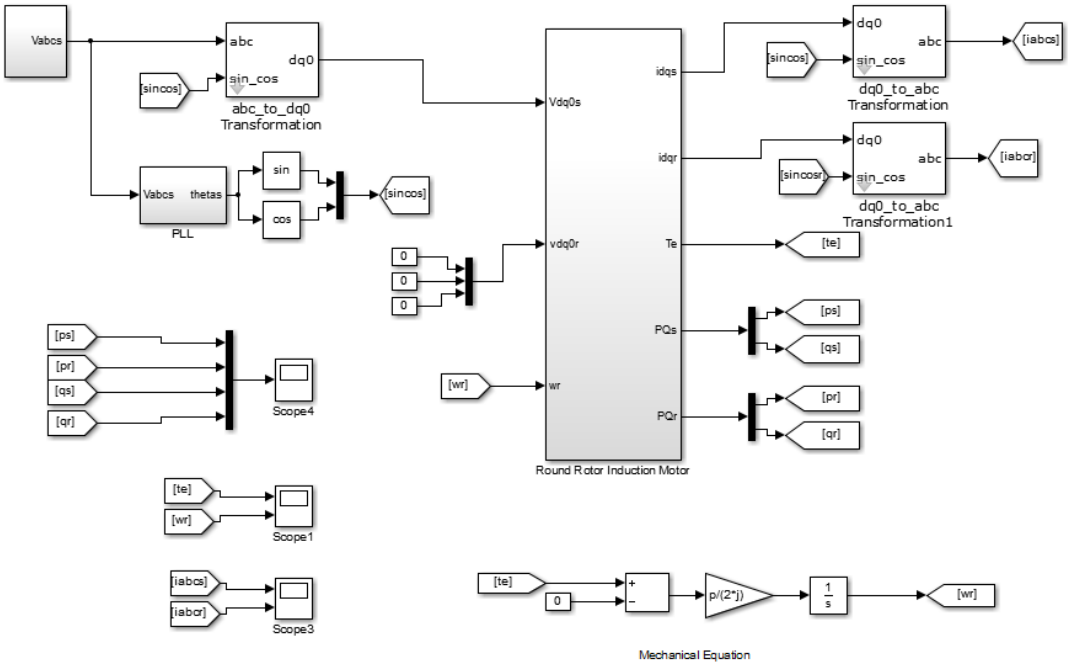

Figure 2.3. Round Rotor Induction Machine Simulation Model

The details of subsystem ‘Round Rotor Induction Motor’ in Figure 2.3 is shown in Figure 2.4. All the equations are solved using ‘Embedded Matlab Function’ block. To test the simulation model, parameters from table 2.1 are simulated. Torque and power calculation box solve equations(86)(88)(89). Rated three phase sinusoidal voltage is applied to the induction motor and its speed torque characteristics are plotted in Figure 2.5 to validate the simulation results.

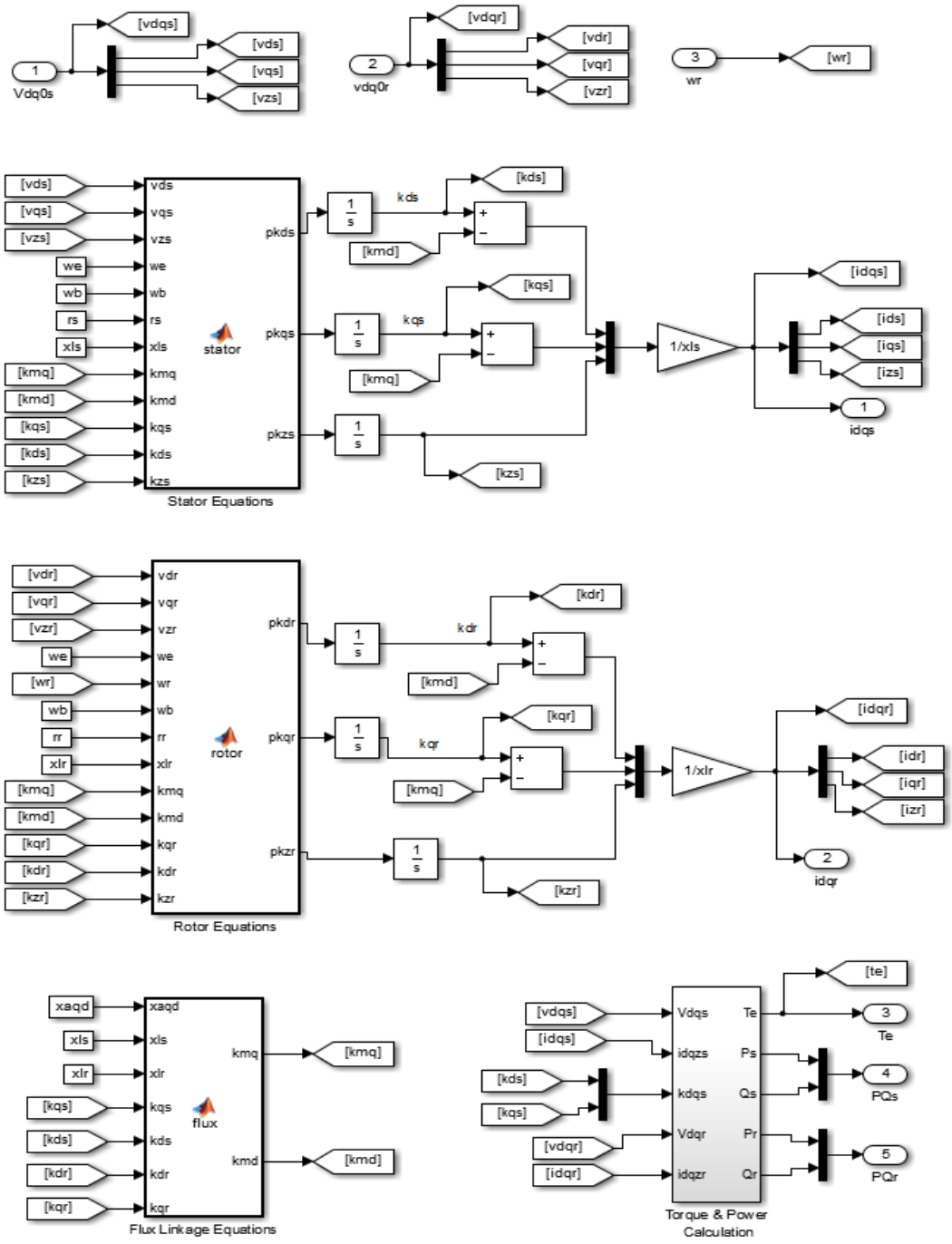

Figure 2.4. Round Rotor Induction Motor Machine Subsystem

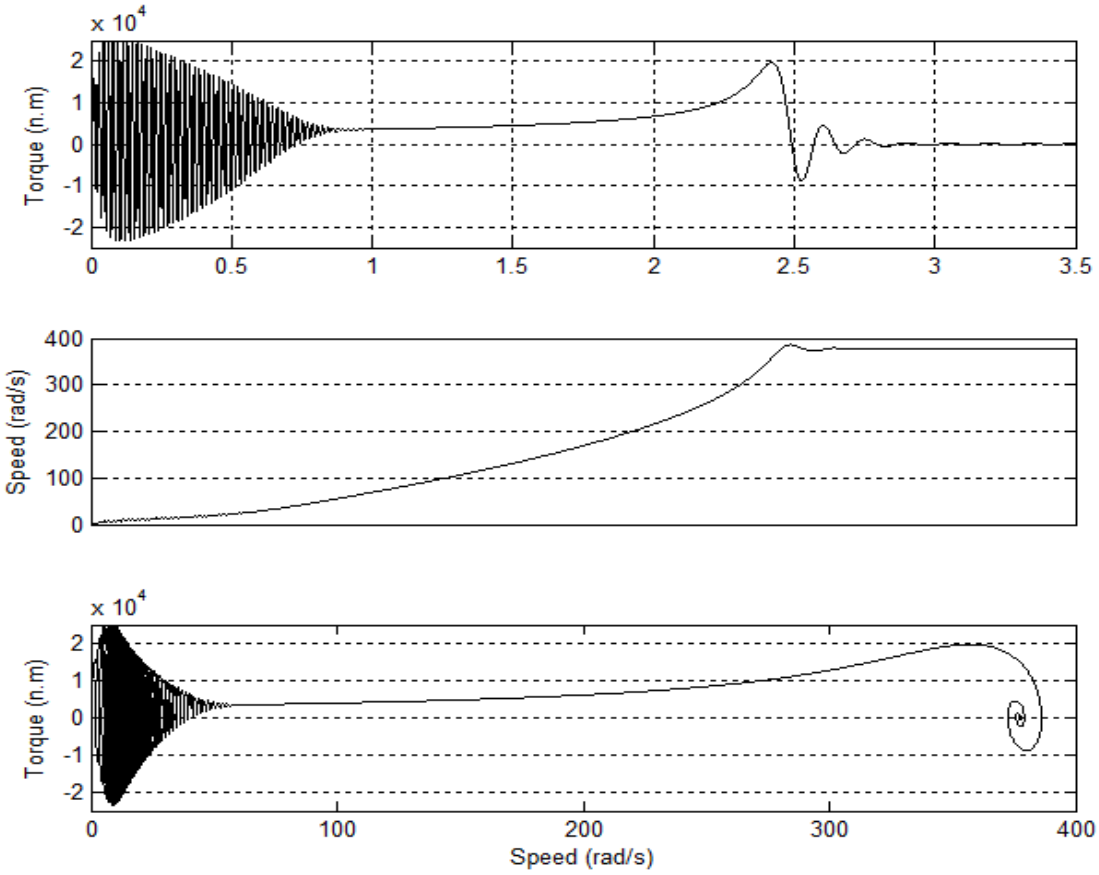

Figure 2.5. Simulation Results for Machine Described in Table 2.1

3. MULTIPLE REFERENCE FRAME THEORY FOR HARMONIC CALCULATION

3.1. LITERATURE SURVEY

The multiple reference frame (MRF) theory has been used mostly for the analysis of different machines in the literature but sometimes it has also been used for the control of harmonic currents. The multiple reference frame estimator (MRFE) can be readily applied to any situation where voltage or current harmonics have to be injected [10].

Some of the earliest papers on multiple reference frame theory by P. Krause have discussed the analysis of the steady state modes of unbalanced or non-sinusoidal operation of a symmetrical induction machine using the multiple reference frame theory [11]. Another paper by P. Krause et. al. established a straightforward method of calculating variables in a rectifier inverter drive system by using multiple reference frames [12]. S. Sudhoff analyzed a multistack variable-reluctance stepper motor using the MRF theory [13]. While P.L. Chapman et. al. employed multiple reference frame theory to analyze a non-sinusoidal brushless DC drive [14].

P. Chapman and S. Sudhoff proposed a synchronous regulator to accurately track three phase commands with arbitrary balanced harmonic content. The proposed regulator uses the multiple reference frame theory to obtain both harmonic estimator as well as feedback controller [10]. S. Lee and S. Su in their paper presented an active filter with a new method of current regulation by using the multiple reference frame theory to calculate the compensating harmonic current in each reference frame [15]. P. Xiao et al. have employed multiple reference frames to develop a selective harmonic compensation method to control three phase PWM boost converters [16]. By using the MRF estimator it

is possible to calculate and compensate the significant harmonics in the current. In this thesis, a specific method of harmonic compensation, based on the multiple reference frame theory is detailed.

3.2. MULTIPLE REFERENCE FRAME HARMONIC OBSERVER

The main objective of this thesis is to calculate the exact current harmonics in the grid and not to limit the compensation to only 5^{th} and 7^{th} harmonics. The harmonics in the grid are measured by using a multiple reference frame harmonic observer. New multiple reference frame synchronous estimator/regulator (MRFSER) was set forth by P. Chapman and S. Sudhoff [10] for the optimal control of permanent magnet synchronous machine drives. The harmonic observer in this thesis is based on MRFER which calculates and tracks harmonics by implementing a series of reference frames for the grid current. Each reference frame is set to track the harmonic or multiple of the fundamental frequency of the grid current using transformation equations.

The *abc* current variables represented by i_{abc} are transformed to the *qd0* variables in each corresponding harmonic reference frame by

$$i_{qd0}^{n} = K^{n} i_{abc} \tag{90}$$

where i_{abc} is a vector consisting of phase currents i_a, i_b, i_c as

$$i_{abc} = \begin{bmatrix} i_a \\ i_b \\ i_c \end{bmatrix} \tag{91}$$

and components of the phase current in any reference frame n is denoted by

$$i_{qd0}^{n} = \begin{bmatrix} i_q^n \\ i_d^n \\ i_0^n \end{bmatrix} \tag{92}$$

also the transformation matrix K^n is as follows

$$K^n = \frac{2}{3}\begin{bmatrix} \cos(n\theta_e) & \cos\left(n\left(\theta_e - \frac{2\pi}{3}\right)\right) & \cos\left(n\left(\theta_e + \frac{2\pi}{3}\right)\right) \\ sin(n\theta_e) & \sin\left(n\left(\theta_e - \frac{2\pi}{3}\right)\right) & \sin\left(n\left(\theta_e + \frac{2\pi}{3}\right)\right) \\ \frac{1}{2} & \frac{1}{2} & \frac{1}{2} \end{bmatrix} \tag{93}$$

where θ_e is the electrical angle of the a-phase utility voltage which is used for calculating the variables in the synchronous reference frame.

$$(K^n)^{-1} = \begin{bmatrix} \cos(n\theta_e) & sin(n\theta_e) & 1 \\ \cos\left(n\left(\theta_e - \frac{2\pi}{3}\right)\right) & \sin\left(n\left(\theta_e - \frac{2\pi}{3}\right)\right) & 1 \\ \cos\left(n\left(\theta_e + \frac{2\pi}{3}\right)\right) & \sin\left(n\left(\theta_e + \frac{2\pi}{3}\right)\right) & 1 \end{bmatrix} \tag{94}$$

The value of n in (93) and (94) will give the qd0 components of the current in the n^{th} reference frame. The value of n can be set to any multiple of fundamental electrical frequency, but as seen in the literature major concerns in electric power distribution systems is the amount of relatively large 5^{th}, 7^{th} and 11^{th} harmonics. So the value of *n* in (93) and (94) is modified to isolate the current in the *6n±1* i.e. 5^{th}, 7^{th}, 11^{th}, 13^{th}, 17^{th}, 19^{th} reference frames. Fig. 3.1 shows the block diagram for the multiple reference frame observer, which is the input to the harmonic compensation block.

To find the suitable harmonic current, the multiple reference frames are selected which vary from fundamental frequency to higher order frequencies. The input to the multiple reference frame harmonic observer is the current vector which goes through different transformation matrices to obtain the current in corresponding reference frame. For faster convergence of the harmonic currents, only the corresponding harmonic current is isolated and fed to the harmonic loop for calculation. The isolated harmonic currents are obtained after each low pass filter. The time constant of the low-pass filter (LPF) is optimally adjusted to obtain a fast response and stable output without any oscillations [16]. Thus this observer is employed for the separation of all the harmonic components in the grid current.

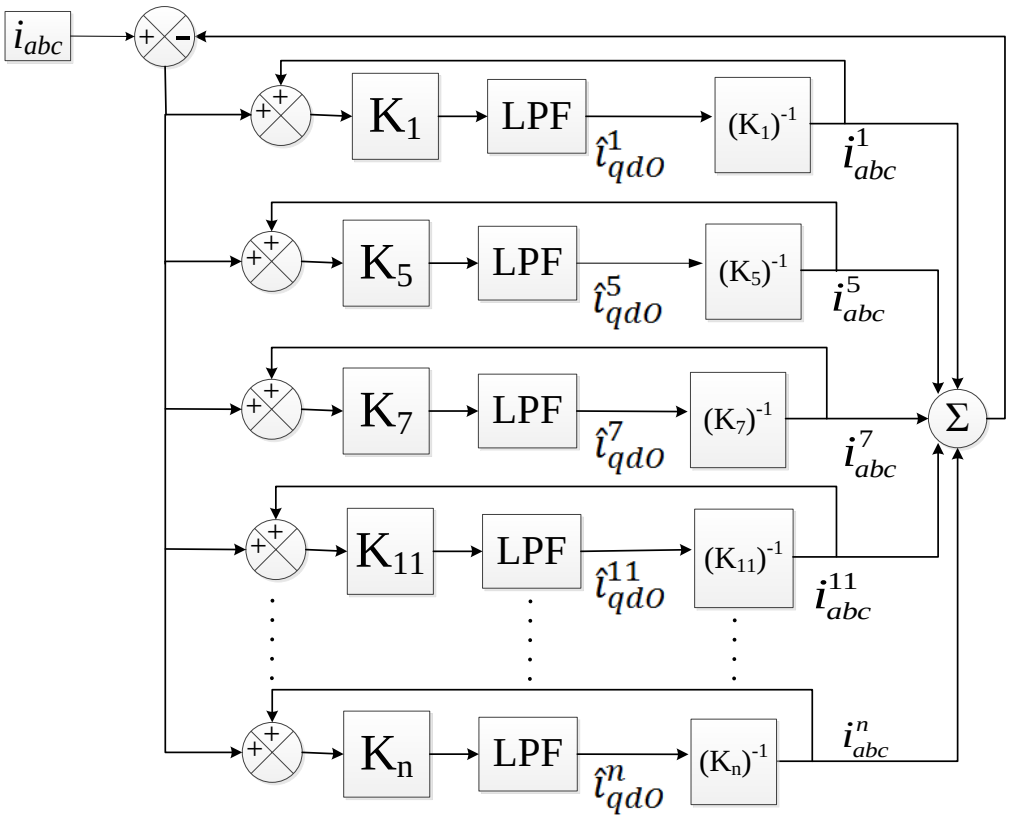

Figure 3.1. Multiple Reference Frame Harmonic Observer [17]

3.3. SIMULATION FOR MRFHO

The simulation of Multiple Reference Frame Harmonic Observer is implemented in the software package Matlab® Simulink®. The doubly-fed induction machine is modeled as discussed in Section 2. It is supplying power to a nonlinear load. The current harmonics due to this load are calculated using the Multiple Reference Frame Harmonic Observer as shown in Figure 3.1. The values calculated from the observer are then compared with the values obtained from the Fourier spectrum of the PLECS scope.

Inputs for the calculations of the observer are the grid current and electrical angle θ_s of the a-phase grid current. This angle is required for transformation equations. A phase locked loop (PLL) is implemented to calculate the electrical angle of the a-phase. The PLL which is implemented in this simulation is as shown in Figure 3.2. The value of θ_s is limited to 0 to 6.28, so the integrator has to be reset after the output crosses 6.28.

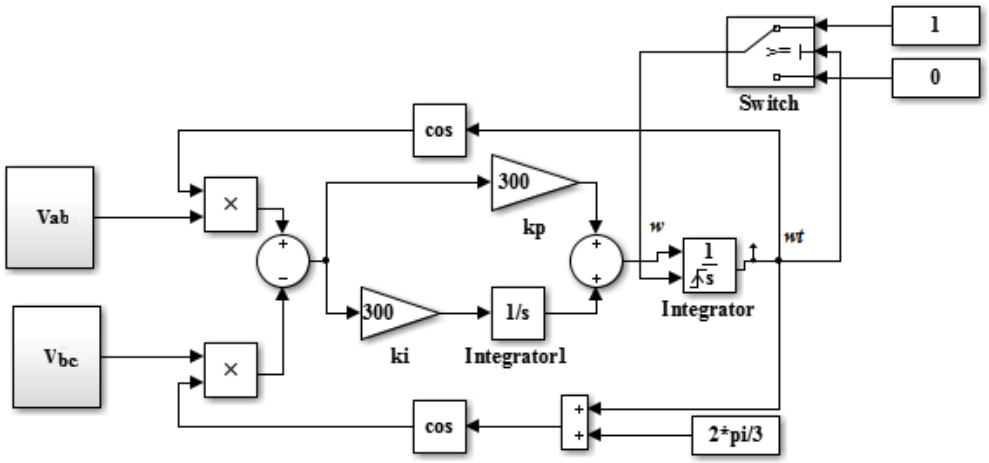

Figure 3.2. Simulink Model for PLL implementation

A Simulink subsystem is designed to model each loop of the MRFHO as shown in Figure 3.3. So to track any particular harmonic, a subsystem is added with harmonic number and θ_s as the input. Each of these subsystems includes matrix calculations for reference frame transformations and a low pass filter. Using such multiple subsystems, the MRFHO is designed as shown in Figure 3.4.

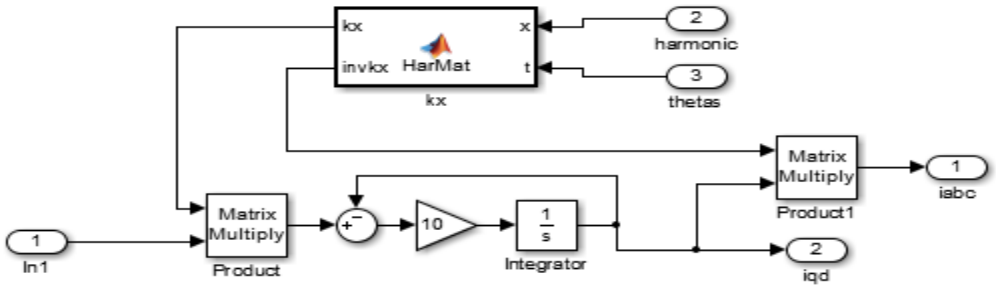

Figure 3.3. Simulation Subsystem Model for Each Loop of MRFHE

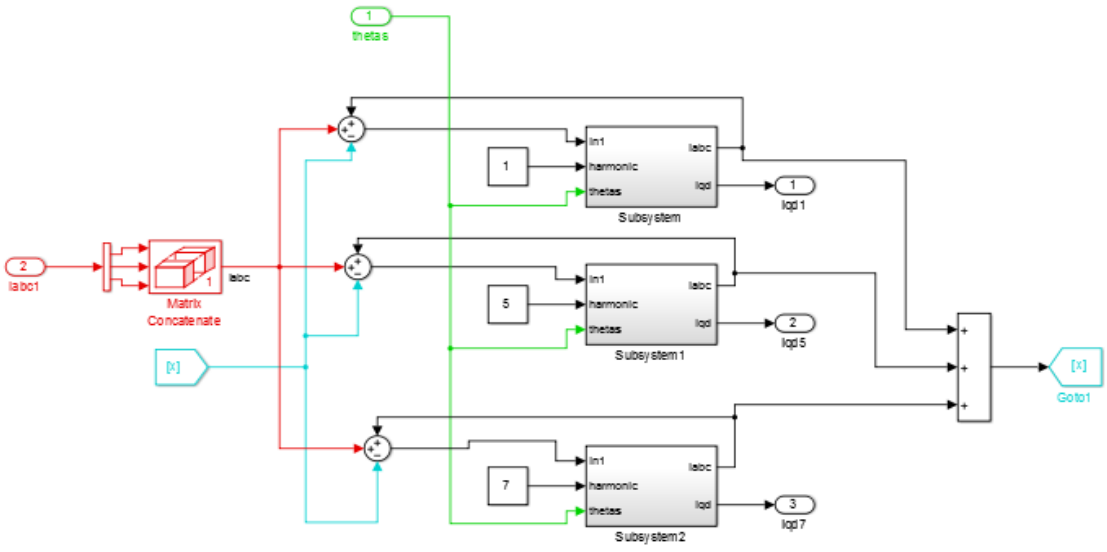

Figure 3.4. Simulation Model for MRFHO

Depending on the harmonics to be calculated, the MRFHO is modeled. In this thesis, the harmonics measured are 5^{th}, 7^{th}, 11^{th}, 13^{th}, 17^{th} and 19^{th}. The complete Simulink model is as shown in Figure 3.5.

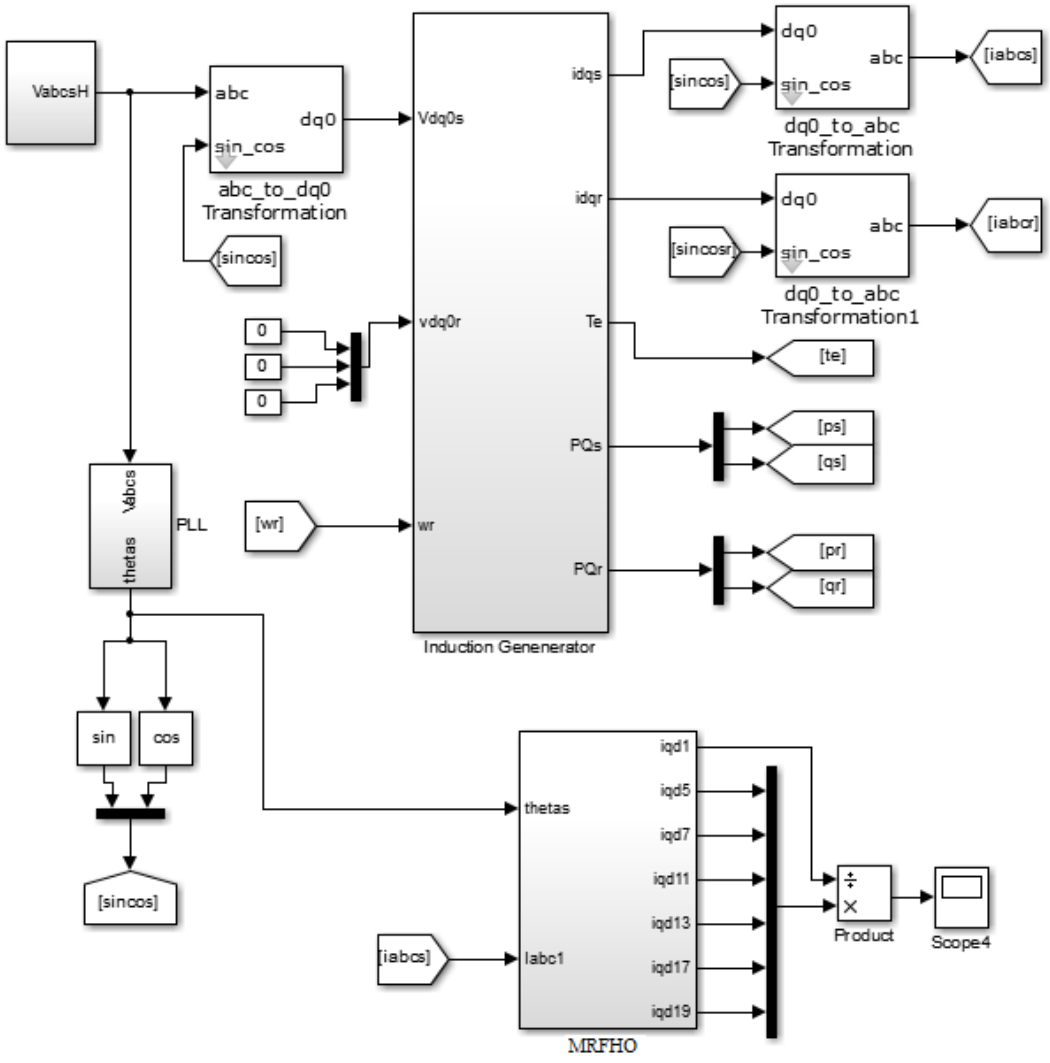

Figure 3.5. Simulation Model for Calculating System Harmonics

3.3.1. Simulation Results for Case 1. Two cases are simulated to demonstrate the effectiveness of the MRFHO.

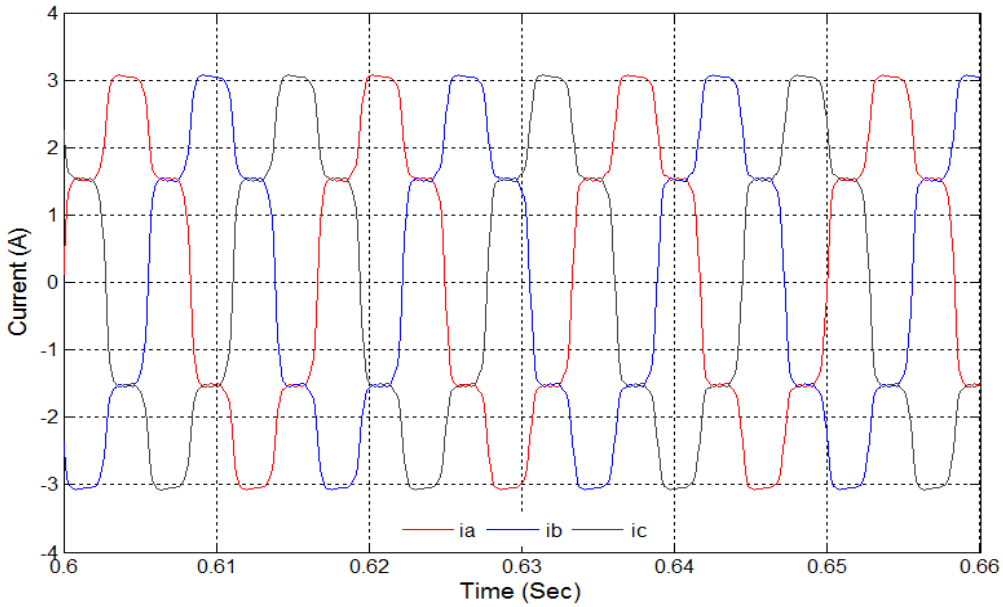

Figure 3.6. Current i_{abc} Before Compensation (Case 1)

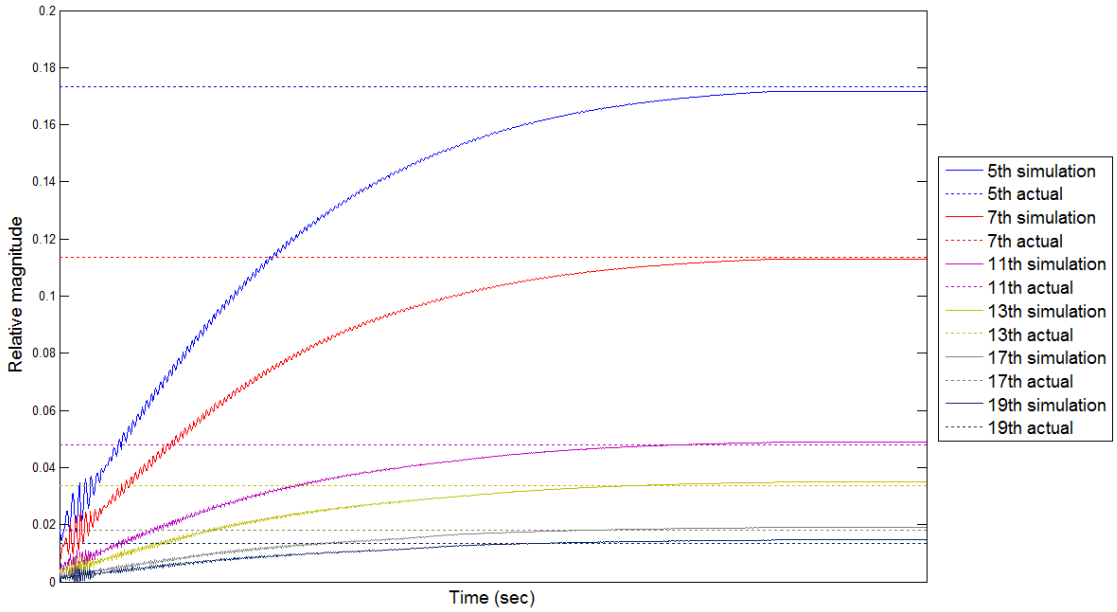

Figure 3.7. Output of Multiple Reference Frame Harmonic Observer (Case 1)

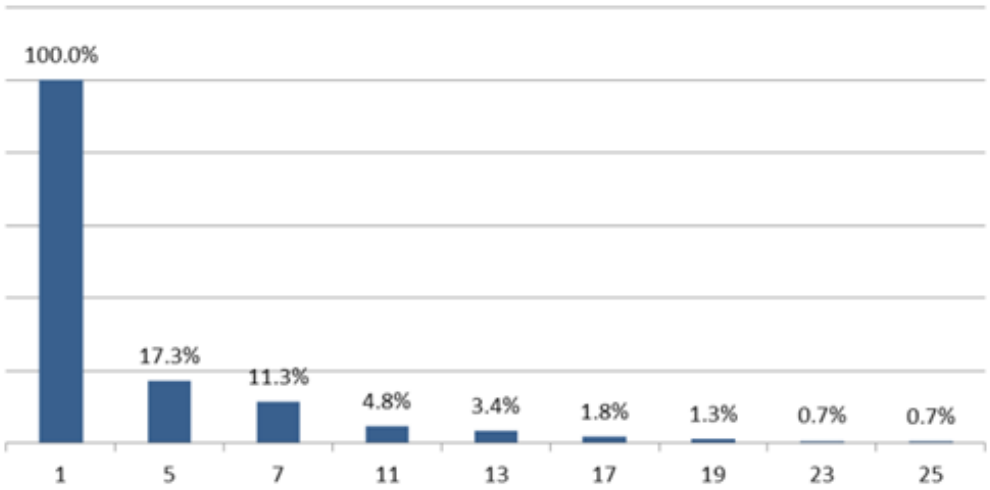

Figure 3.8. Current Harmonics Calculated by Fourier Spectrum (Case 1)

3.3.2. Simulation Results for Case 2.

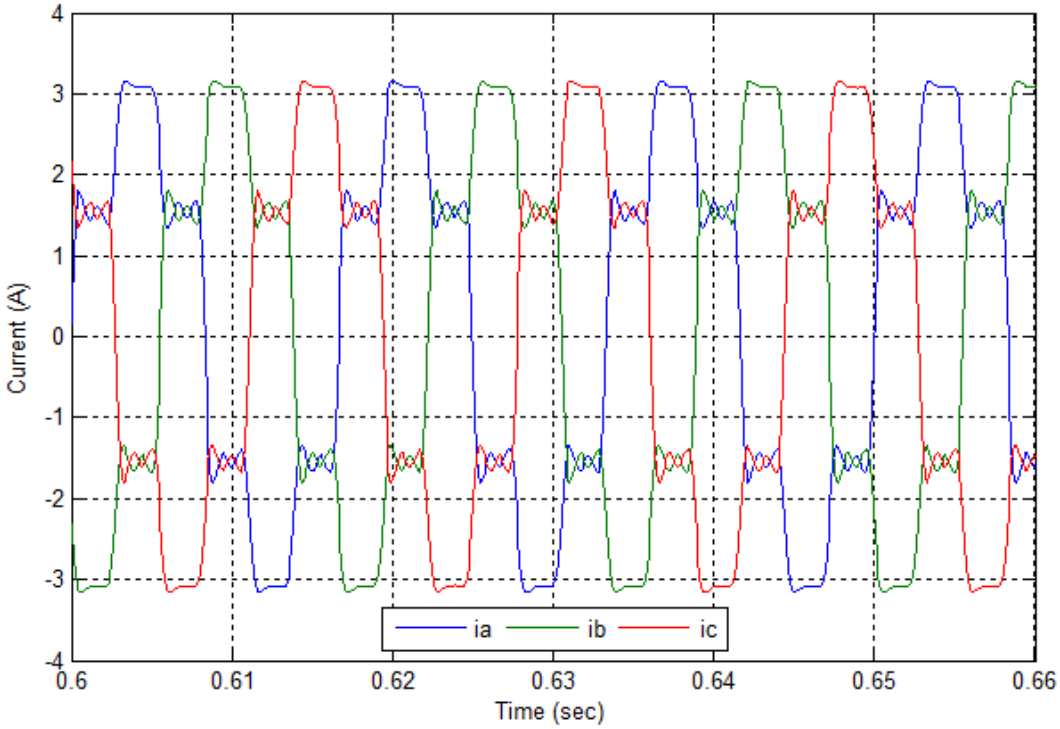

Figure 3.9. Current i_{abc} Before Compensation (Case 2)

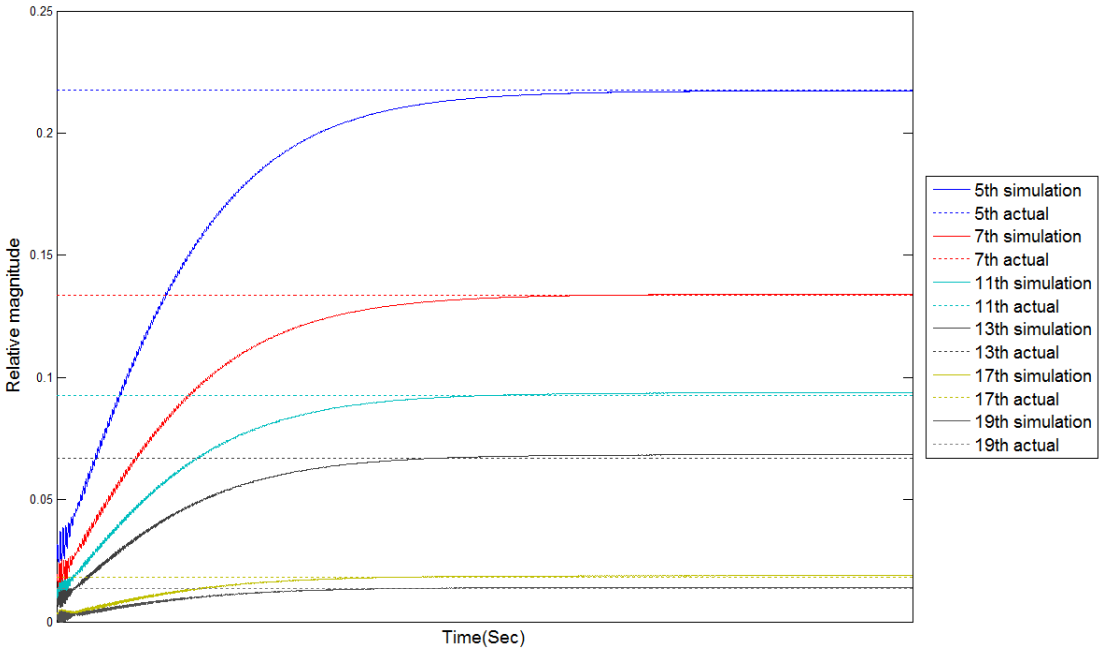

Figure 3.10. Output of Multiple Reference Frame Harmonic Observer (Case 2)

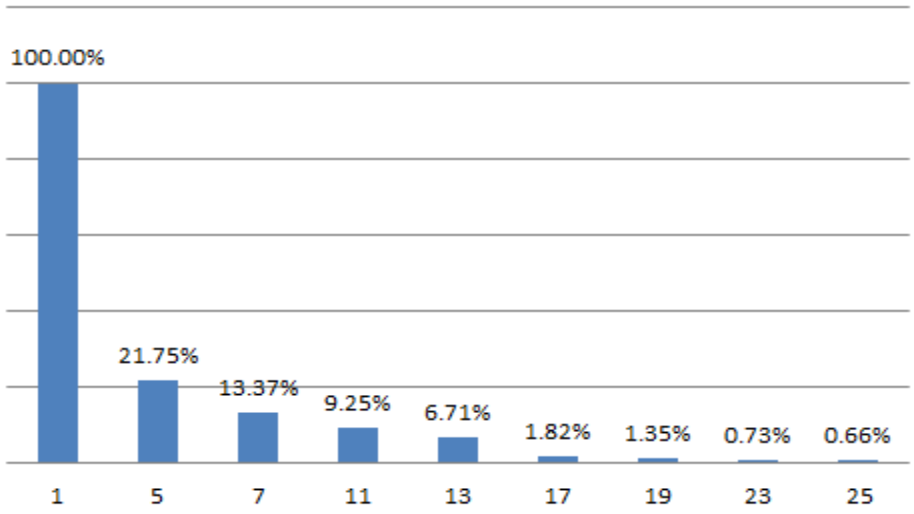

Figure 3.11. Current Harmonics Calculated by Fourier Spectrum (Case 2)

Results of case 1 and 2 show the accuracy of MRFHO. It takes few milliseconds for each subsystem to the settle at the harmonic distortion value in the input current.

3.4. DSP IMPLEMENTATION OF MRFHO

The Texas Instruments TMS320F28335 digital signal processor has been used to implement the MRFHO. DSP uses the analog to digital converter (ADC) blocks to measure grid voltage and load current and calculate actual parameters. The line voltages are fed to the PLL to calculate the a-phase angle or θ_s. Using θ_s and i_a, i_b, i_c, current in each reference frame is calculated. Using CAN communication the real time calculated values of currents in each of 5^{th}, 7^{th}, 11^{th}, 13^{th} reference frame can be observed on the computer using the software Vector® CANoe®. The DSP code is generated using Embedded Coder and Simulink in Matlab. The simulation model in section 3.3 is modified for implementation on DSP.

3.4.1. Sensor Board and Signal Conditioning Circuit. The sensor board consists of voltage and current measuring circuits. The line voltages V_{ab}, V_{bc}, V_{ca} required for the PLL are measured using an LEM LV25-P sensor. This circuit is designed to measure voltages of 0-300V. The voltage to be measured is connected at V_1 and V_2 terminals. The sensor requires a voltage input of +15V and -15V for operation. The output voltage from terminal M is further connected to the signal conditioning board. The value of R1 in the measuring circuit is chosen as 75 kΩ. Voltage measuring circuit is as shown in Figure 3.12. Three of such circuits are used to measure the three line to line voltages.

Similarly line currents i_a, i_b, and i_c are measured using an LEM LA 55-P hall effect transducer. A load wire is passed through the sensor to carry the current in the direction as shown on the sensor. Output terminal M is connected to the signal

conditioning board. Three of the circuits as shown in Figure 3.13 are used to measure the three line currents.

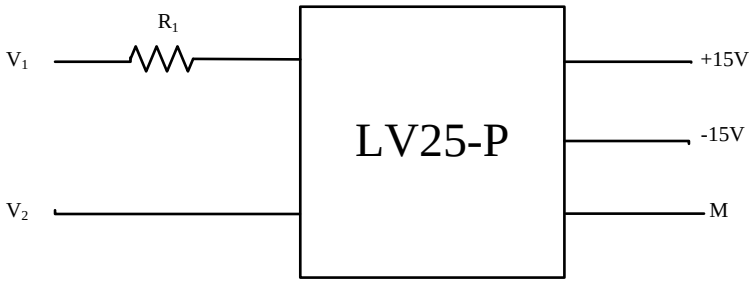

Figure 3.12. Voltage Measuring Circuit

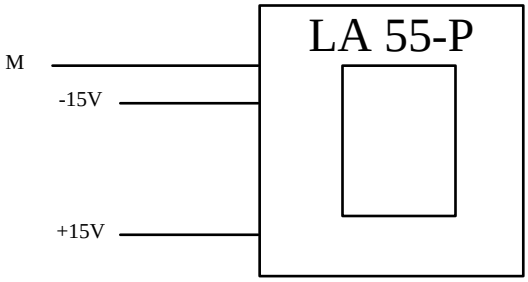

Figure 3.13. Current Measuring Circuit

The output of the current and voltage sensors is between -3.3V and +3.3V. But the ADC of DSP can only measure positive voltages with respect to its ground. So a voltage conditioning circuit has to be installed to convert to the required voltage ratings. Block diagram for the Signal Conditioning Circuit is shown in Figure 3.14.

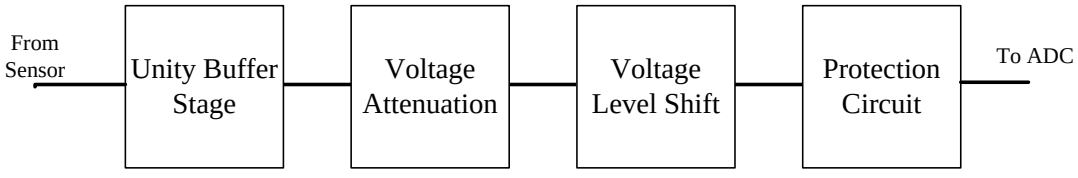

Figure 3.14. Signal Conditioning Circuit Block Diagram

The circuit is designed to shift, attenuate, and provide buffer to input signal. Op-amp ST LF347 which is a quad J-FET operational amplifier is used in this circuit. While in operation, when no signal is applied, the voltage output of the conditioning circuit is 1.5V. Each of six sensors (3 voltage, 3 current sensors) use such voltages conditioning circuit.

3.4.2. Sensor Calibration. The ADC block of the DSP reads the value of the voltage or current in binary. To convert this binary value to an actual signal value, the sensors have to be calibrated. Also, the sensors and the signal conditioning circuit add some gain and some fixed DC bias. To accurately calibrate the sensors, a precision multimeter and a good variable DC supply are used. A DC value is applied across the sensor and the corresponding value by the DSP is measured via CAN. Numbers of readings are recorded and a graph of input voltage vs. DSP reading is plotted for each sensor. The signal conditioning board adds a fixed a 1.5V. So when no voltage is applied across the sensors the DSP value is 2048.

3.4.3. CAN Communication. To observe the real time DSP calculations, the variables are communicated via CAN bus using the software Vector CANoe and Vector CANcaseXL box. A database file is created which consists of the signals which are to be observed. These signals are then packed in message. Proper hardware setup has to be done before programming the DSP. High, low and ground pins from CAN transreceiver on the DSP have to be connected to the corresponding pins on the Vector CANcaseXL box.

3.4.4. DSP coding. The DSP coding in this thesis is done using 'Embedded Coder' block set in Matlab Simulink. A discrete time simulation model is built, compiled and the C-code is generated. The simulation model is shown in the Figure 3.15.

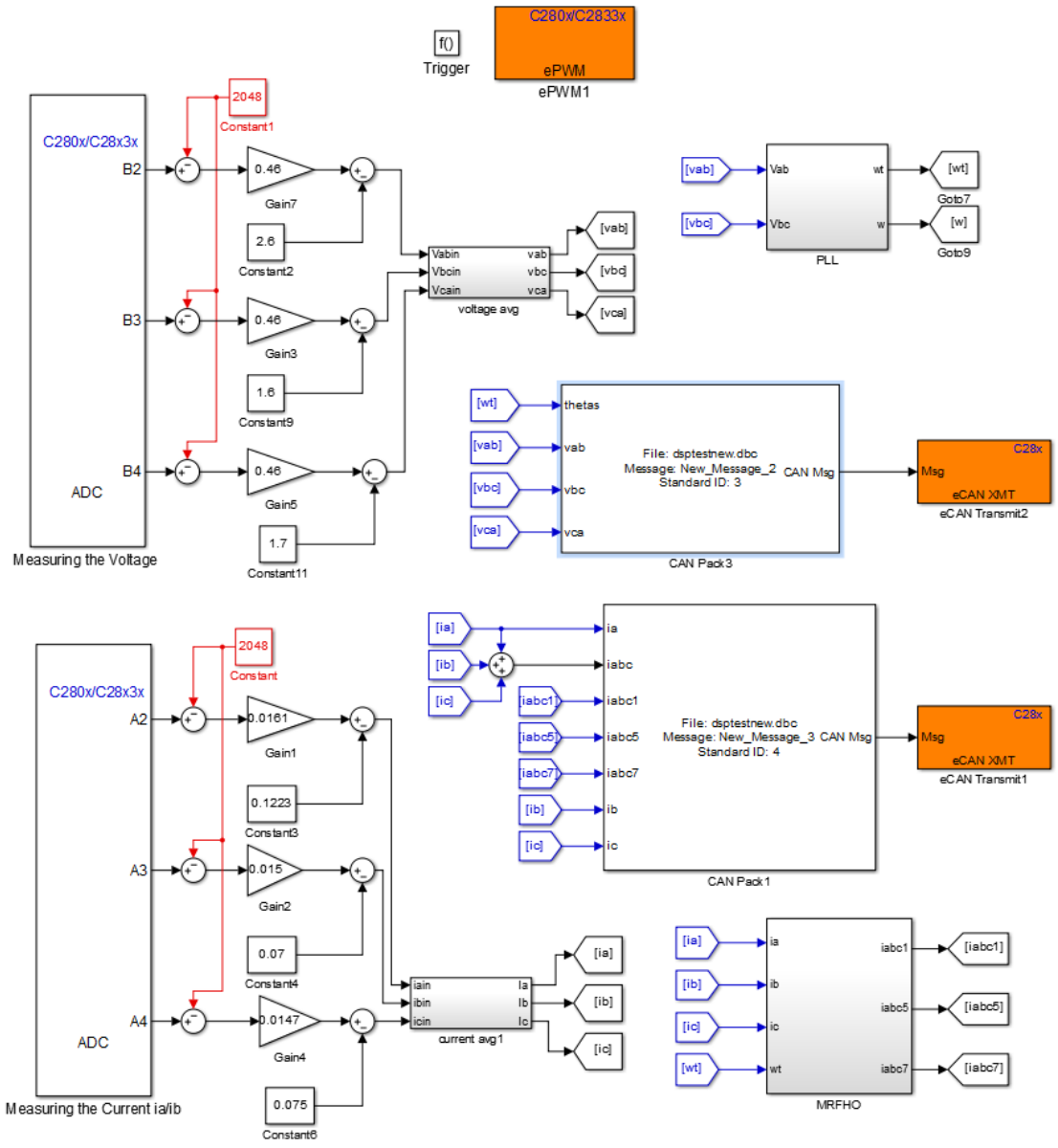

Figure 3.15. Simulink Model for DSP Implementation

The simulation model in Section 3.3 is modified from continuous time domain to discrete time domain. All the transfer functions and operations in s-domain are converted to z-domain. So all the integrators and low pass filters (LPF) used in the MRFHO were converted to equivalent discrete domain integrators and z-domain LPFs. Other changes included the ADC blocks for the input of the grid voltage and current.

The inputs to the subsystem 'PLL' are voltages v_{ab} and v_{bc}. The output of this subsystem is the a-phase angle and θ_s. Subsystem 'MRFHO' calculates the value of current in each reference frame. It is modeled as per simulation Figure 3.4. In this model, currents from the 5th and 7th harmonic frame are calculated. The 'CAN pack' and 'eCAN transmit' blocks are used for packing the CAN message and transmitting it over the CAN bus.

The inputs from the sensors are first scaled to their actual values and then to get smooth waves average of 5 previous values is performed for each ADC output. The subsystem for averaging is as shown in Figure 3.16. Averaging is done for both current as well as voltage.

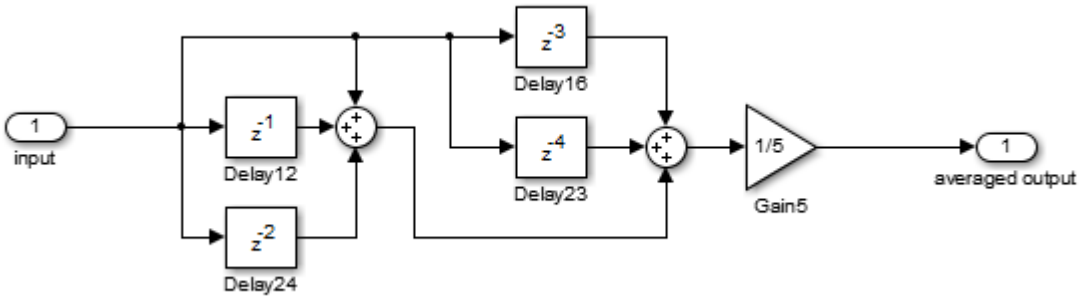

Figure 3.16. DSP Averaging Subsystem

3.4.5. Hardware Setup. Three current and three voltage sensors measure parameters for all 3-phases. The output of the sensor board is connected to the signal conditioning board which is further connected to ADC pins of the DSP. The DSP is also connected to the computer for burning the code using Code Composer Studio. For testing the code for the MRFHO on DSP, a non-linear load is created in the laboratory using Elgar programmable power supply. The hardware setup is as shown in Figure 3.17.

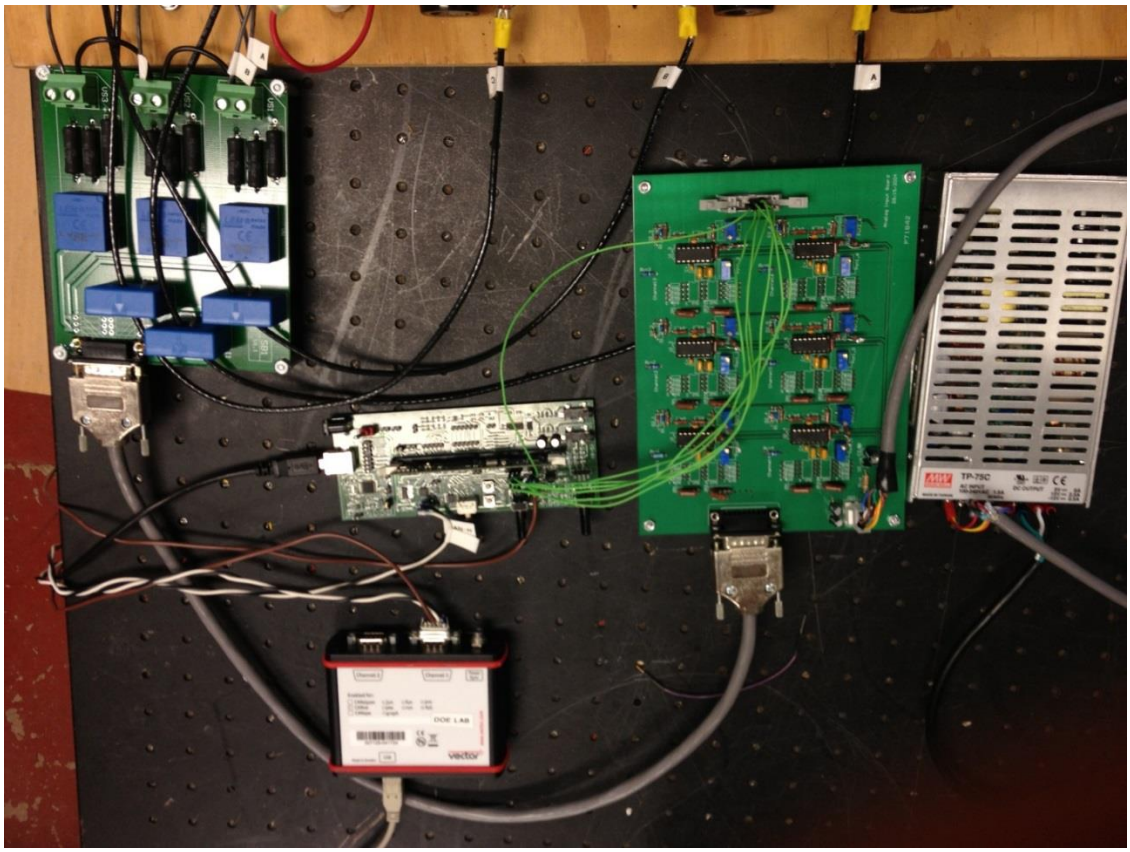

Figure 3.17. Experimental Hardware Setup

3.4.6. Results. Figure 3.18 the voltage sensor readings converted to actual voltage values. The PLL output shows that it exactly tracks the a-phase voltage

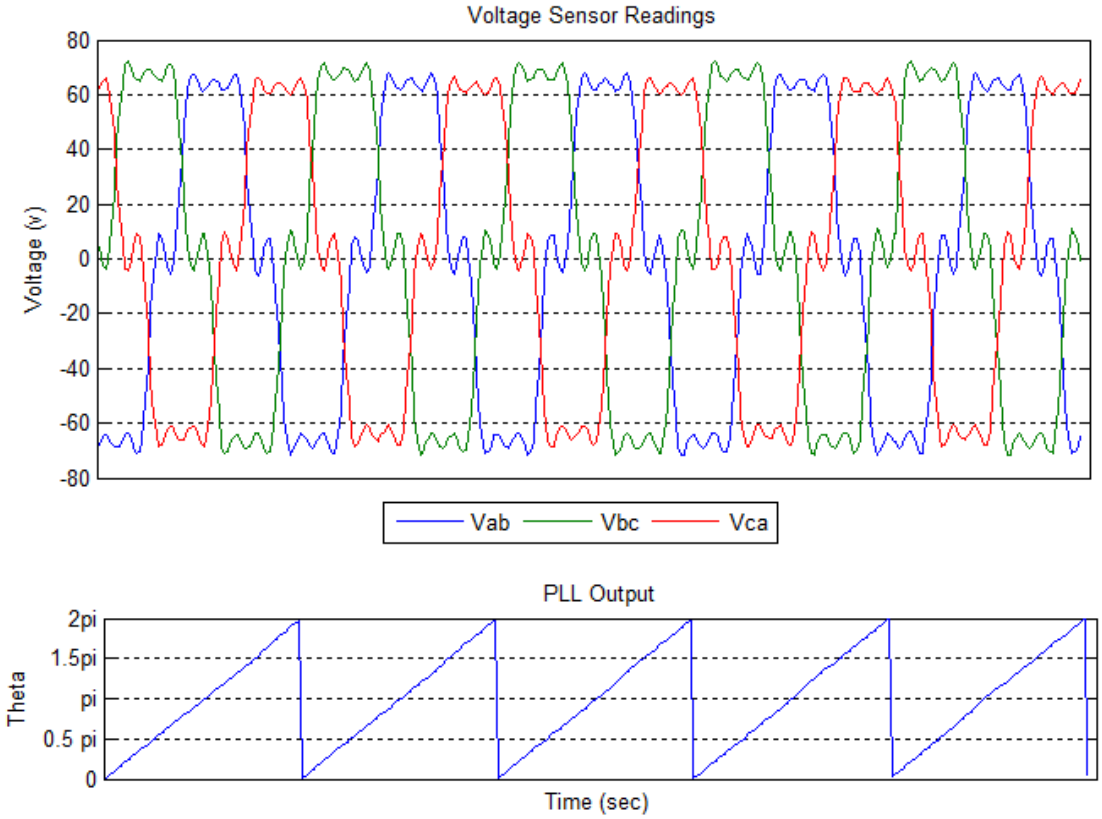

Figure 3.18. Voltage Sensor and PLL output

Table 3.1 lists the harmonics (of the order 1-12) present in the current as measured by the scope Tektronix MSO4034. Both the relative magnitude and actual rms value of the current are calculated. The DSP calculates the value of the current in the 5^{th} and 7^{th} reference frame of the fundamental frequency. The readings are very close and thus the DSP code is able to separate the harmonics in the current.

Table 3.1. Comparison of Scope and DSP Readings

	Tektronix MSO4034			DSP Readings	
Harmonic number	**Frequency**	**Mag**	**Mag RMS**	**Mag**	**Mag RMS**
	Hz	**%**	**A**	**%**	**A**
1	59.99	100.00%	0.301328	100.00%	0.275168
2	119.98	0.28%	0.000837		
3	179.97	0.69%	0.002083		
4	239.96	0.09%	0.000275		
5	299.95	20.05%	0.060419	19.50%	0.05366
6	359.94	0.22%	0.000665		
7	419.93	14.17%	0.042707	13.01%	0.035786
8	479.93	0.15%	0.000446		
9	539.92	0.41%	0.001221		
10	599.91	0.04%	0.000132		
11	659.90	0.38%	0.001142		
12	719.89	0.21%	0.000635		
13	779.88	0.44%	0.001316		

4. HARMONIC COMPENSATION VIA DFIG

4.1. LITERATURE SURVEY

Various methods have been employed in the literature for harmonic compensation. Tremblay et al. have compensated harmonics by absorbing the harmonics in the grid side converter of the DFIG [18]. Another method is discussed for using a shunt active filter for wind turbine generators [19].

For developing an algorithm for DFIG based harmonic compensation, main focus of the research is based on the method which calculates the harmonics in the system. Gaillard et al. have calculated the harmonics by tuning a high selectivity based harmonic isolator [20], while Abolhassani et al. presented a sensorless flux oriented vector control method for harmonic compensation in addition to the control of active and reactive power [21, 22]. Kairous uses a control approach based on sliding mode control for power generation control and compensation of harmonic currents [23].

Hence it is possible to eliminate significant harmonic currents in a grid by employing a proper rotor side current control.

4.2. PREDICTABLE HARMONIC COMPENSATION

As seen from the literature along with active and reactive power generation, DFIG based wind generators has the capability to maintain a high level of power quality by canceling the most significant and troublesome harmonic currents of the utility grid. To compensate harmonics present in the grid via DFIG, specific currents have to be injected in the rotor. The block diagram for the predictable harmonic compensation is shown in Figure 4.1. There is a nonlinear load in the system which injects harmonics. The

harmonics created by the load in the model contain only the 5^{th} harmonic. The magnitude of the 5^{th} harmonic is known and does not change during the simulation time.

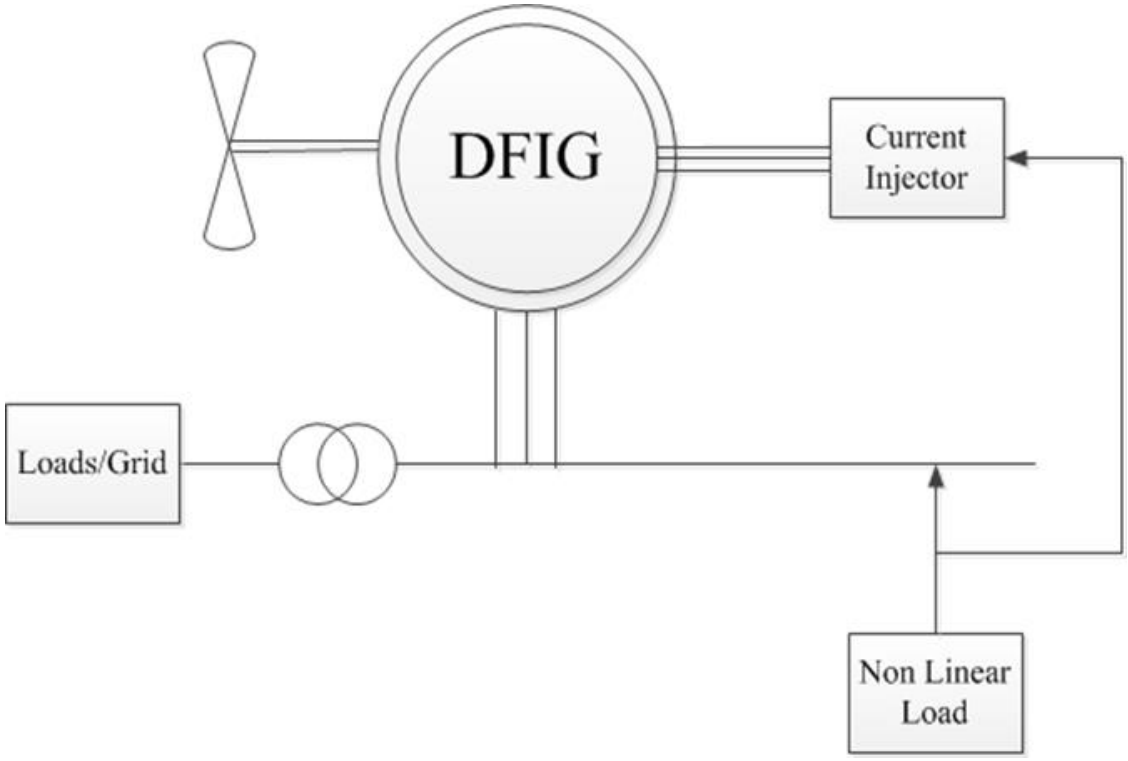

Figure 4.1. Block Diagram for Predictable Harmonic Compensation

To compensate for the 5^{th} harmonic, -6^{th} harmonic current has to be injected in the rotor. Similarly to compensate for the 7^{th} harmonic, 6^{th} harmonic current has to be injected in the rotor. So to mitigate harmonics in the current system, -6^{th} harmonic current with the same magnitude is generated and injected in the rotor of the DFIG. Figure 4.2 shows the a-phase voltage, which contains 5^{th} harmonic along with the fundamental frequency. Figure 4.3 shows, the compensation of the harmonics. This simulation shows that if the magnitude and the order of harmonics are known then any harmonics in the system can be compensated via a DFIG.

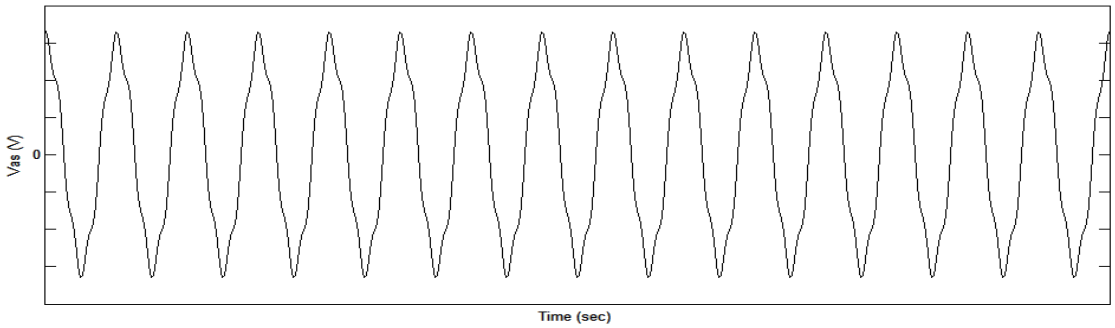

Figure 4.2. Harmonic Voltage Waveform in the System

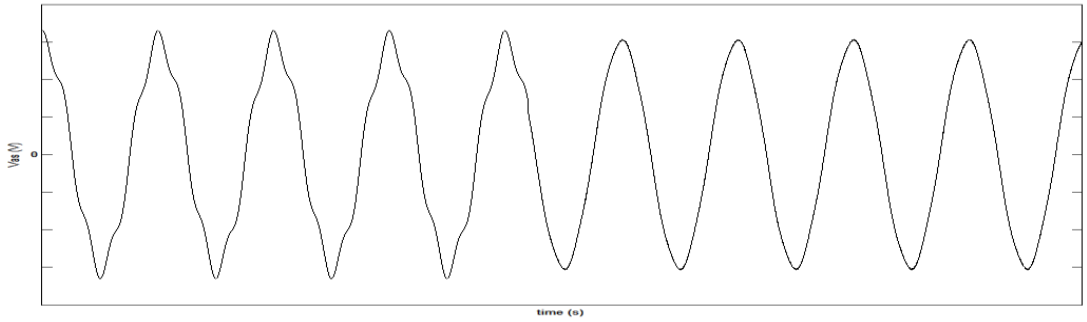

Figure 4.3. Voltage Waveform after Compensation

4.3. MRFHO BASED HARMONIC COMPENSATION SYSTEM FOR DFIG

The magnitude and order of the harmonic should be known to compensate any harmonic in the system. This calculation can be done using a MRFHO. To compensate all odd harmonics (6n-1), -6n harmonic current has to be injected in the rotor and to compensate all even harmonics (6n+1), 6n harmonic current has to be injected. Figure 4.4 shows the system where the DFIG is employed as a harmonic compensator. The stator of the DFIG is connected to the grid which contains system loads and some nonlinear loads; corrupting the grid power. A phase-locked-loop (PLL) is implemented to calculate the electrical angle of the a-phase utility voltage θ_s. The rotor side converter is used to inject the harmonics into the rotor

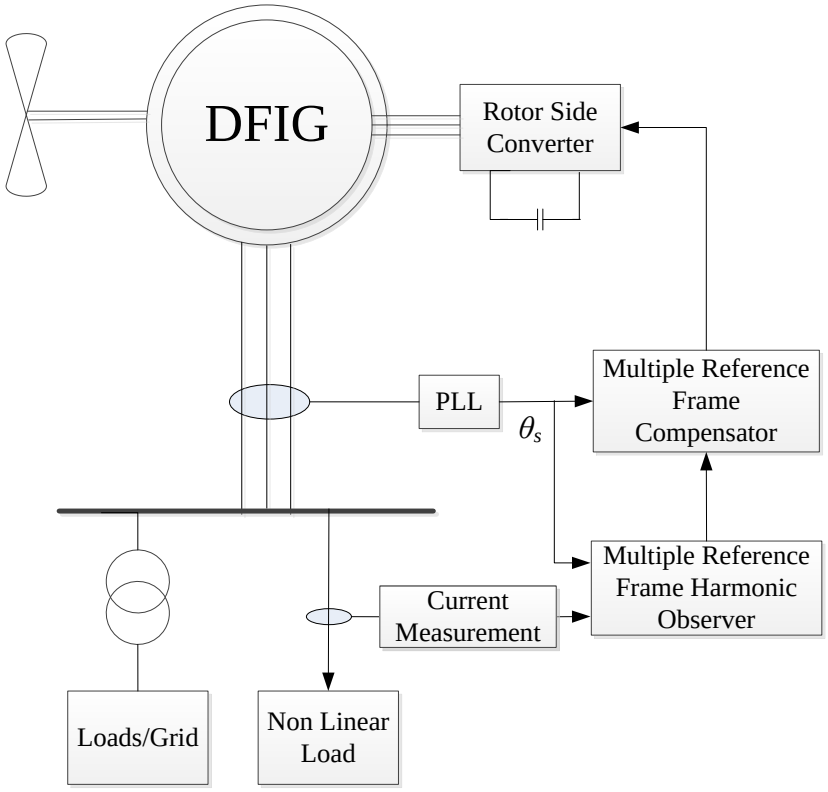

Figure 4.4. Block Diagram for the DFIG Harmonic Compensation System

The block ‘Multiple Reference Frame Harmonic Compensator’ reconstructs the waveforms to be injected in the rotor using magnitude from the MRFHO and angle from the PLL as inputs. This output acts as a reference current for the rotor side converter (RSC). Hysteresis control can be used for the RSC to generate the current injected in the rotor. The grid side converter (GSC) is used to keep the voltage across the DC link capacitor constant. In this simulation, GSC is modeled as a constant DC supply. In this simulation 5^{th}, 7^{th}, 11^{th}, 13^{th}, 17^{th} and 19^{th} harmonics are mitigated. The simulation model for the DFIG based harmonic compensation system appears in Figure 4.5.

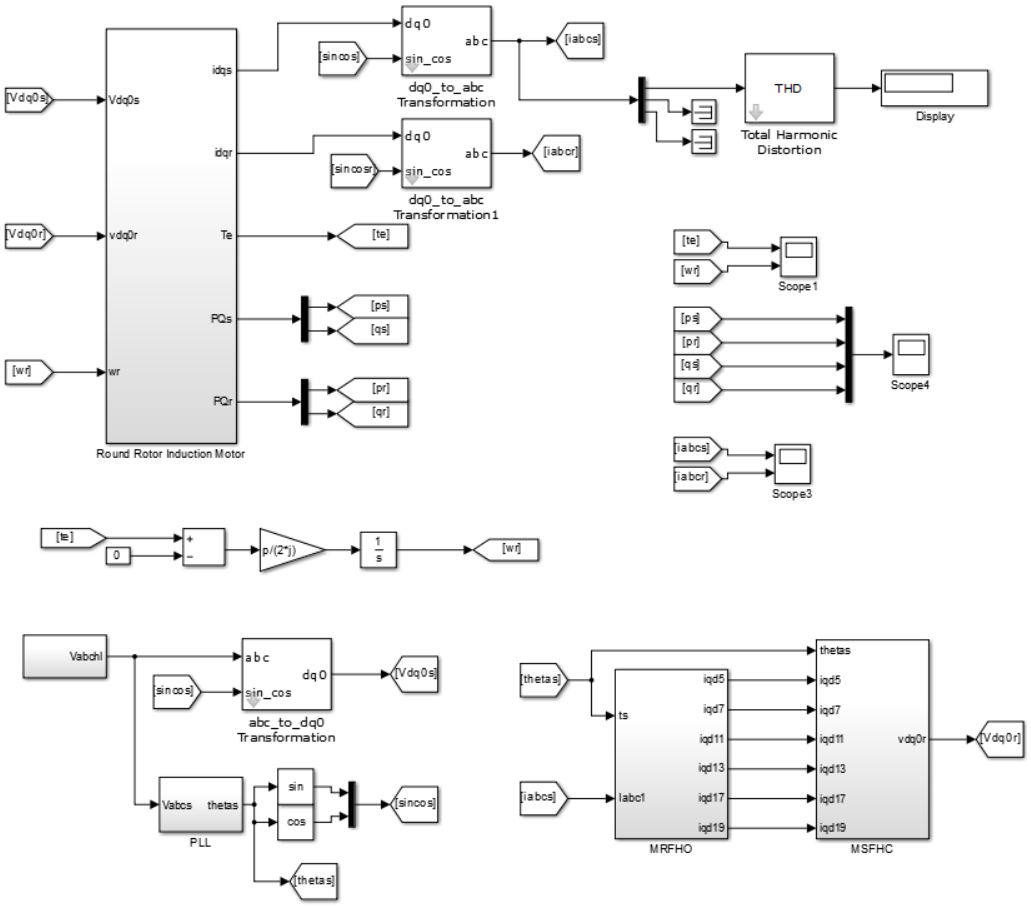

Figure 4.5. Simulation Model for the DFIG Based Harmonic Compensation System

4.4. SIMULATION RESULTS

The harmonics detected in Case 1 of chapter 3.3.1 are compensated. Figure 4.6 shows the stator current after compensation. Figure 4.7 shows the Fourier spectrum of the stator current after compensation.

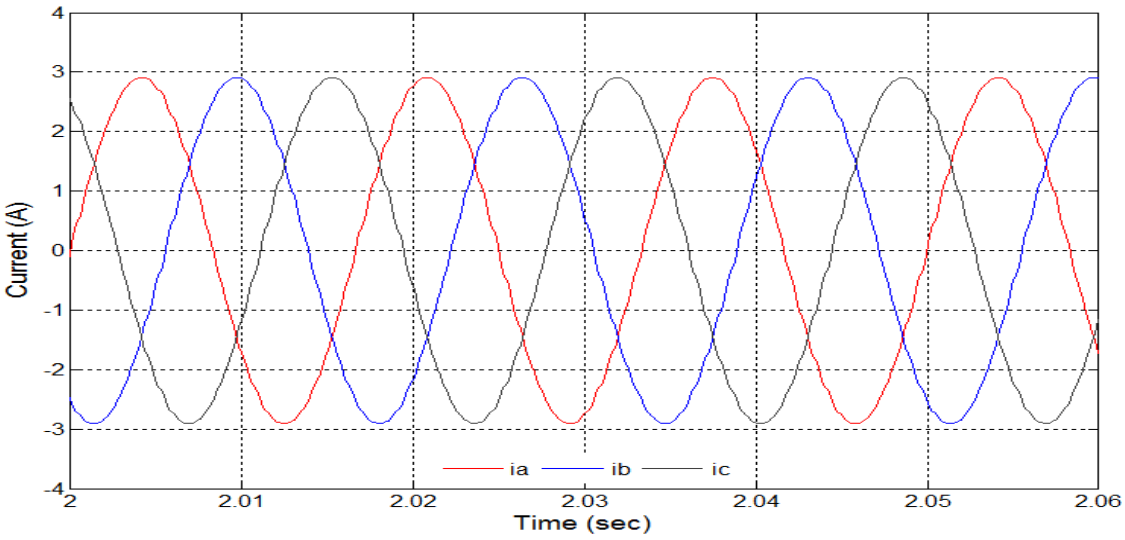

Figure 4.6. Current after Compensation

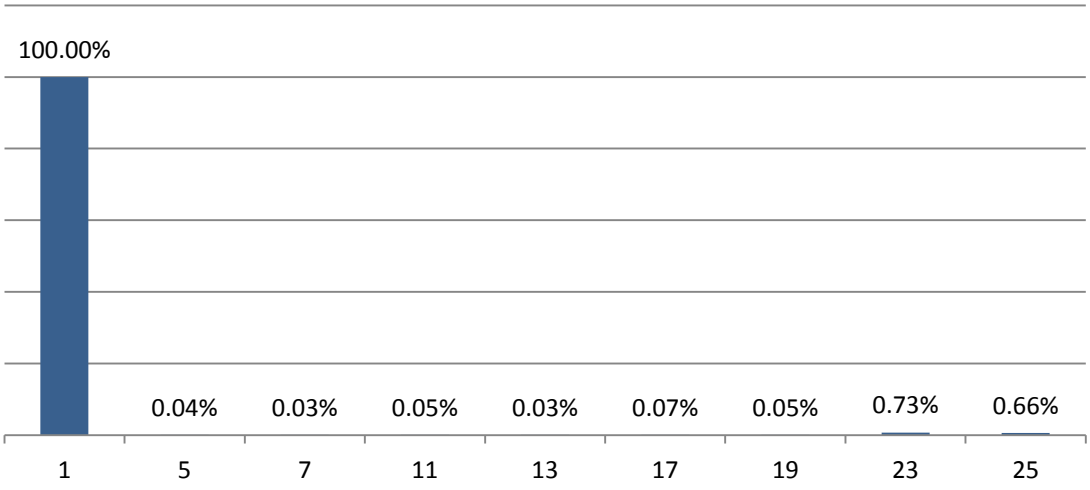

Figure 4.7. Current Harmonics Calculated by Fourier Spectrum

Table 4.1 compares the harmonic currents in the system before and after compensation. The targeted harmonics, i.e. 5^{th}, 7^{th}, 11^{th}, 13^{th}, 17^{th} and 19^{th} are almost eliminated from the system.

Table 4.1. Current Harmonics in the System

Harmonic	Before Compensation	After Compensation
1	100%	100%
5	17.33%	0.04%
7	11.35%	0.03%
11	4.78%	0.05%
13	3.35%	0.03%
17	1.82%	0.07%
19	1.35%	0.05%
23	0.73%	0.73%
25	0.66%	0.66%

5. SIMULTANEOUS ACTIVE AND REACTIVE POWER COMPENSATION ALONG WITH HARMONIC MITIGATION

The primary objective of the DFIG based wind generation system is to generate active and reactive power. A lot of research has been conducted to develop independent control of active and reactive power drawn from DFIG. R. Pena et al. put forth an idea of vector control for rotor side converter for variable input rotor speed [24], while Abolhassani et al. propose a vector control method without a position sensor [22]. Chowdhury et al. in their paper use a stator flux oriented control method to obtain simulation and experimental results [25].

For the independent control of active and reactive power, equations (44)-(46) and (50)-(55) are substituted with flux linkage equations and rearranged to solve for stator current

$$\begin{bmatrix} I_{qs}^{e} \\ I_{ds}^{e} \end{bmatrix} = \begin{bmatrix} r_s & \omega_e L_{ss} \\ -\omega_e L_{ss} & r_s \end{bmatrix}^{-1} \begin{bmatrix} v_{qs}^{e} - \omega_e L_M I_{dr}^{'e} \\ v_{ds}^{e} + \omega_e L_M I_{qr}^{'e} \end{bmatrix} \tag{95}$$

It is assumed that $\omega_e L_{ss} >> r_s$ and in Synchronous reference frame,

$$v_{qs}^{e} = \sqrt{2} V_s \ \& \ v_{qs}^{e} = 0$$

$$I_{qs}^{e} \approx -\frac{L_M}{L_{ss}} I_{qr}^{'e}$$

$$I_{ds}^{e} \approx \frac{\sqrt{2} V_s}{\omega_e L_{ss}} - \frac{L_M}{L_{ss}} I_{dr}^{'e}$$

Substituting above parameters in the stator active, reactive power equations (88) and (89)

$$P_s = -\frac{3}{2}\sqrt{2}V_s i_{qs}^e \approx \frac{3}{2}\frac{\sqrt{2}V_s L_M}{L_{ss}} I_{qr}^{'e} \tag{96}$$

$$Q_s = -\frac{3}{2}\sqrt{2}V_s i_{ds}^e \approx \frac{3}{2}\frac{\sqrt{2}V_s L_M}{L_{ss}} I_{dr}^{'e} - \frac{V_s^2}{\omega_e L_{ss}} \tag{97}$$

From equation (96), the stator active power can be controlled by q-axis rotor current in synchronous reference frame and from (97), the reactive power can be controlled by d-axis rotor current in synchronous reference frame. If harmonic number to the MRFHO is given to be one, it will calculate q and d axis currents in the synchronous reference frame. The sum of reference current for power control and harmonic compensation is used as the reference for rotor side converter. This method can give both independent active, reactive power control, as well as harmonic mitigation. Figure 5.1 shows the simulation diagram for simultaneous active reactive power control and harmonic compensation.

The parameters of induction machine used for the simulation of simultaneous active and reactive power are given in the Table 5.1.

Table 5.1. Induction Machine Parameters [9]

Power (HP)	Power (KW)	Volts	rpm	T_B (N.m)	I_B (amps)
2250	1678	2300	1786	8900	421.2
r_s (Ω)	X_{ls} (Ω)	X_m (Ω)	$X_{lr}^{'}$ (Ω)	$r_r^{'}$ (Ω)	J (kg.m^2)
0.029	0.226	13.04	0.226	0.022	63.87

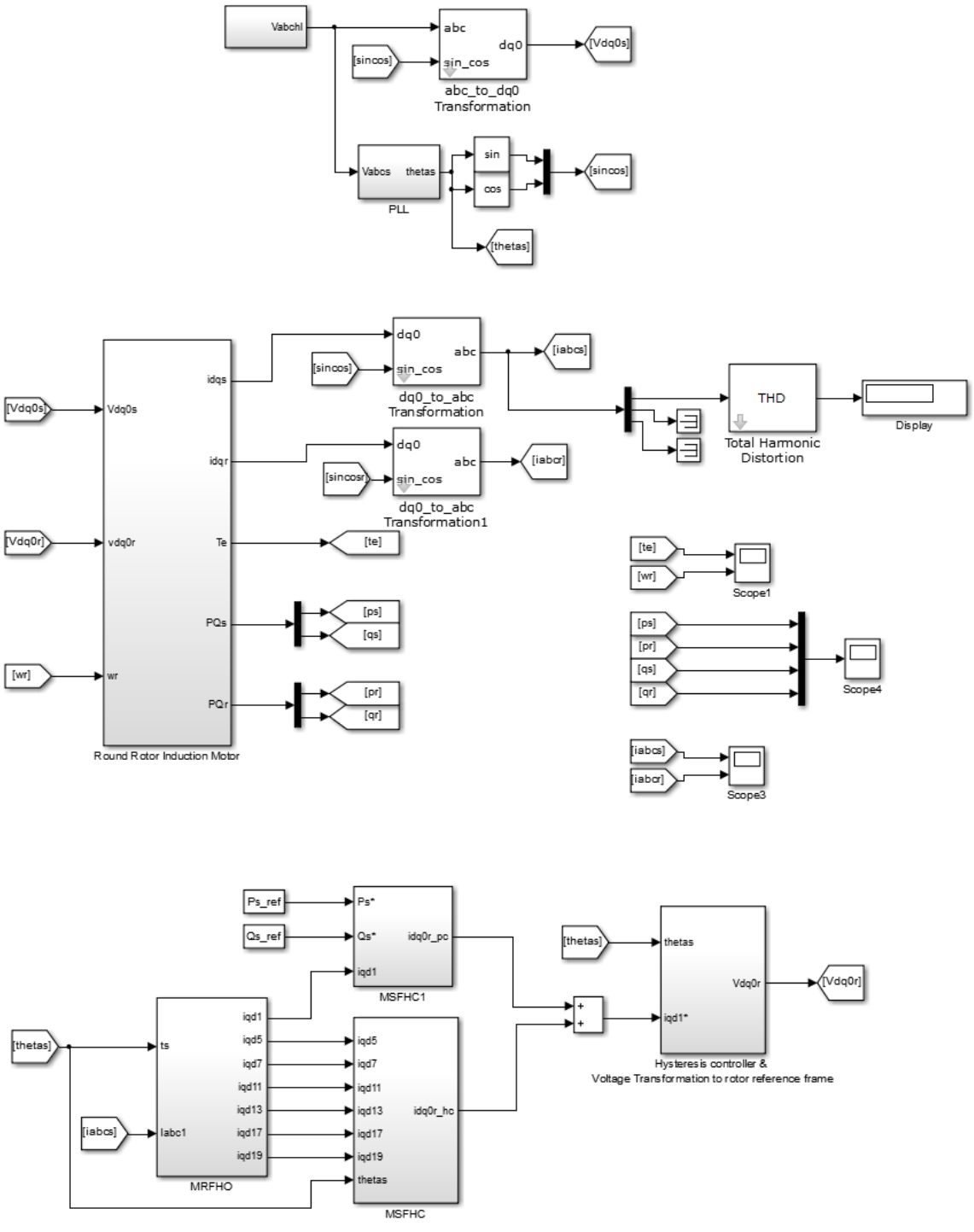

Figure 5.1. Simulation Diagram for Simultaneous Active, Reactive Power Control and Harmonic compensation

To see the effect of variable rotor speed on active and reactive power generations, the rotor speed is steadily varied ramped from 75% of synchronous speed or 1350 rpm to 125% of synchronous speed or 2250 rpm. The reference for this simulation was 1.6 MW for active power and 0 MW for reactive power. Figure 5.2 shows the simulation results for variable rotor speed. The stator active and reactive power is constant as rotor speed is varied. But the rotor active and reactive power is variable. The rotor absorbs the power when the rotor speed is less than synchronous speed while it delivers power when the rotor speed is greater than synchronous speed. Simulation results for rotor speed of 1350 rpm and 2250 rpm are illustrated in Figures 5.3 and 5.4 respectively.

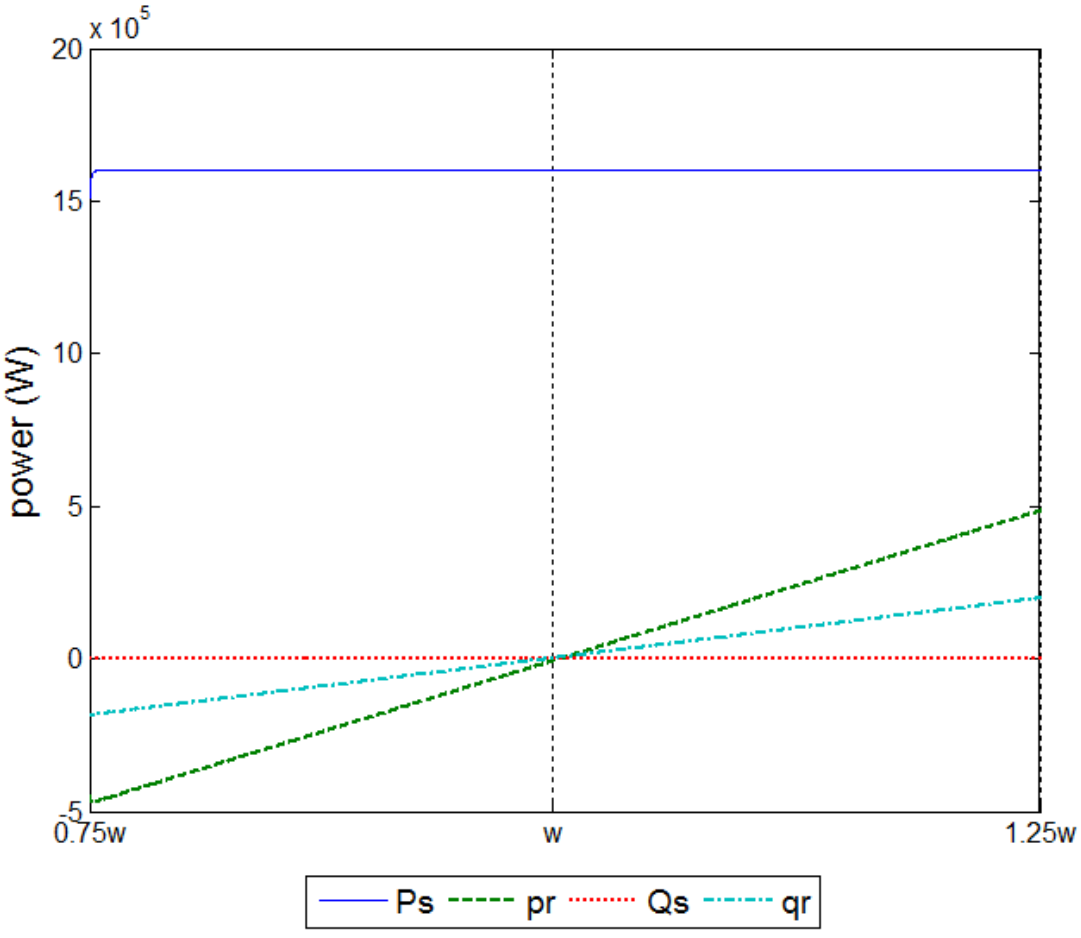

Figure 5.2. Real and Reactive Power Characteristics vs. Rotor Speed

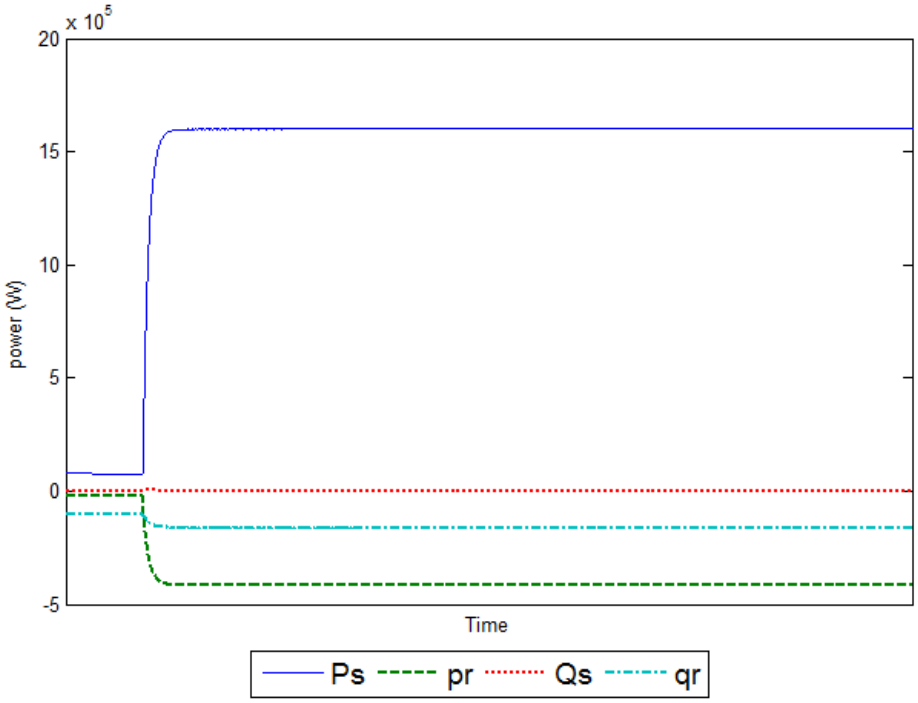

Figure 5.3. Simulation Results for Rotor Speed = 1350rpm

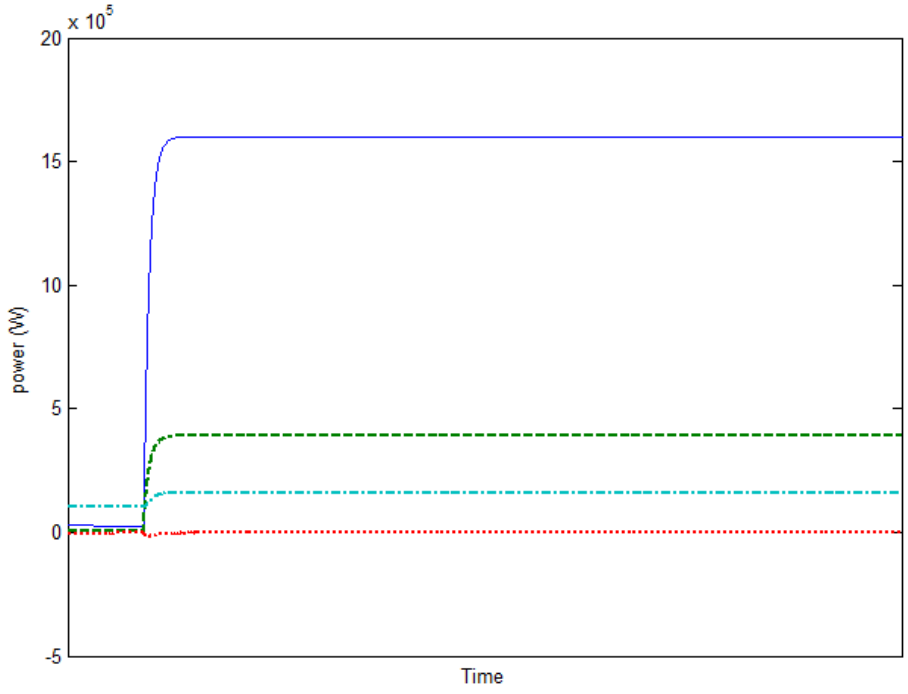

Figure 5.4. Simulation Results for Rotor Speed = 2250rpm

6. CONCLUSION AND FUTURE WORK

In this thesis, a novel method of multiple reference frame based harmonics measurement and compensation technique for doubly-fed induction generators is proposed. This method was later extended for simultaneous and independent control of active and reactive power generation and harmonic compensation.

The multiple reference frame harmonic observer, calculates any required harmonics in the grid accurately. Experimental and simulation results validate the analysis of the observer. Multiple reference frame based harmonic compensation technique is able to compensate the harmonics effectively. Simulation result show that this proposed method is effective in reducing the current harmonics in the system from 21.37% to 0.83% after compensation.

The main advantage of this method is the flexibility to detect and compensate any harmonic in the system. The main limitation of using a DFIG based harmonic filter is that the amount of harmonic filtering is constrained by the rating of the rotor side converter which is generally sized around 25% to 30% of the machine rating.

Future work can involve studying the effects of harmonic injection on stator and rotor windings and overall machine design. Also multiple reference frame theory can be extended to study and solve other DFIG based wind generator problems.

BIBLIOGRAPHY

[1] W. W. E. Association, "World Wind Energy Report 2012," Bonn, GermanyMay 2013.

[2] R. Wiser, Z. Yang, M. Hand, O. Hohmeyer, D. Infield, P. H. Jensen, V. Nikolaev, M. O'Malley, G. Sinden, and A. Zervos, "Wind Energy," in *IPCC Special Report on Renewable Energy Sources and Climate Change Mitigation*, O. Edenhofer, R. Pichs-Madruga, Y. Sokona, K. Seyboth, P. Matschoss, S. Kadner, T. Zwickel, P. Eickemeier, G. Hansen, S. Schlömer, and C. von Stechow, Eds., ed Cambridge, United Kingdom and New York, NY, USA: Cambridge University Press, 2011.

[3] D.-J. B. Henk Polinder, H. Li, Z. Chen, "Concept report on generator topologies, mechanical & electromagnetic optimization," Delft University of Technology, Aalborg University2007.

[4] S. Muller, M. Deicke, and R. W. De Doncker, "Doubly fed induction generator systems for wind turbines," *Industry Applications Magazine, IEEE,* vol. 8, pp. 26-33, 2002.

[5] IEEE, "IEEE Recommended Practices and Requirements for Harmonic Control in Electrical Power Systems," ed, April 12, 1993.

[6] Electromagnetic Compatibility(EMC) - Part 3 Limit 2, "Limits for harmonic current emissions (equipment input current <= 16A per phase," in *IEC 61000-3 Document, First Edition*, ed, 1995.

[7] S. Santoso, *Fundamentals of electric power quality*. Austin, Tex.: Published by Surya Santoso through CreateSpace, 2009.

[8] H. Akagi, "Active Harmonic Filters," *Proceedings of the IEEE*, vol. 93, pp. 2128-2141, 2005.

[9] P. C. Krause, O. Wasynczuk, S. D. Sudhoff, and I. P. E. Society, *Analysis of electric machinery and drive systems*: IEEE Press, 2002.

[10] P. L. Chapman and S. D. Sudhoff, "A multiple reference frame synchronous estimator/regulator," *Energy Conversion, IEEE Transactions on,* vol. 15, pp. 197-202, 2000.

[11] P. C. Krause, "Method of Multiple Reference Frames Applied to the Analysis of Symmetrical Induction Machinery," *Power Apparatus and Systems, IEEE Transactions on,* vol. PAS-87, pp. 218-227, 1968.

[12] P. C. Krause and J. R. Hake, "Method of Multiple Reference Frames Applied to the Analysis of a Rectifier - Inverter Induction Motor Drive," *Power Apparatus and Systems, IEEE Transactions on,* vol. PAS-88, pp. 1635-1641, 1969.

[13] S. D. Sudhoff, "Multiple reference frame analysis of a multistack: variable-reluctance stepper motor," *Energy Conversion, IEEE Transactions on,* vol. 8, pp. 418-424, 1993.

[14] P. L. Chapman, S. D. Sudhoff, and C. A. Whitcomb, "Multiple reference frame analysis of non-sinusoidal brushless DC drives," *Energy Conversion, IEEE Transactions on,* vol. 14, pp. 440-446, 1999.

[15] L. Sang-Joon and S. Seung-Ki, "A harmonic reference frame based current controller for active filter," in *Applied Power Electronics Conference and Exposition, 2000. APEC 2000. Fifteenth Annual IEEE*, 2000, pp. 1073-1078 vol.2.

[16] X. Peng, K. A. Corzine, and G. K. Venayagamoorthy, "Multiple Reference Frame-Based Control of Three-Phase PWM Boost Rectifiers under Unbalanced and Distorted Input Conditions," *Power Electronics, IEEE Transactions on,* vol. 23, pp. 2006-2017, 2008.

[17] O. Ghatpande, K. Corzine, P. Fajri, and M. Ferdowsi, "Multiple reference frame theory for harmonic compensation via doubly fed induction generators," in *Power and Energy Conference at Illinois (PECI), 2013 IEEE*, 2013, pp. 60-64.

[18] E. Tremblay, A. Chandra, and P. J. Lagace, "Grid-side converter control of DFIG wind turbines to enhance power quality of distribution network," in *Power Engineering Society General Meeting, 2006. IEEE*, 2006, p. 6 pp.

[19] F. S. dos Reis, J. A. V. Ale, F. D. Adegas, R. Tonkoski, S. Slan, and K. Tan, "Active Shunt Filter for Harmonic Mitigation in Wind Turbines Generators," in *Power Electronics Specialists Conference, 2006. PESC '06. 37th IEEE*, 2006, pp. 1-6.

[20] A. Gaillard, P. Poure, S. Saadate, and M. Machmoum, "Variable speed DFIG wind energy system for power generation and harmonic current mitigation," *Renewable Energy,* vol. 34, pp. 1545-1553, 2009.

[21] M. T. Abolhassani, P. Enjeti, and T. Hamid, "Integrated Doubly Fed Electric Alternator/Active Filter (IDEA), a Viable Power Quality Solution, for Wind Energy Conversion Systems," *Energy Conversion, IEEE Transactions on,* vol. 23, pp. 642-650, 2008.

[22] M. T. Abolhassani, P. Niazi, H. A. Toliyat, and P. Enjeti, "A sensorless integrated doubly-fed electric alternator/active filter (IDEA) for variable speed wind energy system," in *Industry Applications Conference, 2003. 38th IAS Annual Meeting. Conference Record of the*, 2003, pp. 507-514 vol.1.

[23] D. Kairous, R. Wamkeue, and B. Belmadani, "Towards DFIG control for wind power generation and harmonic current mitigation," in *Electrical and Computer Engineering (CCECE), 2010 23rd Canadian Conference on*, 2010, pp. 1-6.

[24] R. Pena, J. C. Clare, and G. M. Asher, "Doubly fed induction generator using back-to-back PWM converters and its application to variable-speed wind-energy generation," *Electric Power Applications, IEE Proceedings* -, vol. 143, pp. 231-241, 1996.

[25] B. H. Chowdhury and S. Chellapilla, "Double-fed induction generator control for variable speed wind power generation," *Electric Power Systems Research*, vol. 76, pp. 786-800, 2006.

VITA

Omkar Amol Ghatpande was born on May 8th, 1987, in Pune, India. He obtained his Bachelor's Degree in Electrical Engineering in 2009 from University of Pune, India. From August 2009 to July 2011 he worked as a Solution Development Engineer in Energy Services department at Honeywell Automation India Ltd. In August 2011, he joined Missouri University of Science and Technology to pursue Master of Science degree in Electrical Engineering. He served as a graduate teaching assistant for the undergraduate Electromechanics Lab. He received his Masters degree in Electrical Engineering in August 2013.